



UNIVERSITÀ DEGLI STUDI DI PADOVA

Dipartimento di Ingegneria Industriale

Tesi di Laurea Magistrale in Ingegneria Aerospaziale

*Improvement of a low-order panel method by far-field
computation of induced drag for arbitrary non-planar wing
configurations*

Relatore:

Prof. Giampaolo Navarro

Correlatore:

Prof. Marco Antonello

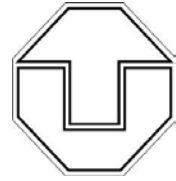
Laureando:

Diego Basso

ANNO ACCADEMICO 2012/2013



**UNIVERSITÀ
DEGLI STUDI DI PADOVA**



e

TECHNISCHE UNIVERSITÄT DRESDEN

Dipartimento di Ingegneria Industriale

Tesi di Laurea Magistrale in
Ingegneria Aerospaziale

***Improvement of a low-order panel method
by far-field computation of induced drag
for arbitrary non-planar wing configurations***

Relatore:

Prof. Giampaolo Navarro

Correlatore:

Prof. Marco Antonello

Laureando:

Diego Basso

ANNO ACCADEMICO 2012/2013

Contents

1	Introduction	1
2	Info About Drag	3
2.1	Drag	3
2.2	Effects of a Finite Wing	6
2.2.1	Downwash	6
2.2.2	Consequences of downwash	7
2.3	Reduction of Induced Drag with Non-Planar Geometry	8
3	Panel Method and Wake Relaxation	11
3.1	Panel Method	11
3.1.1	Formulation	11
3.1.2	Boundary Condition	12
3.1.3	Set of Linear Algebraic Equations	14
3.2	Relaxation Process	16
3.2.1	Points Evaluation	17
4	Induced Drag Calculation	19
4.1	Equation development	19
4.2	Integration of the Induced Drag	24
5	Description of the program	29
5.1	Iteration Process	29
5.1.1	Points Integration	30
5.2	Seeking convergence	30
5.2.1	Geometry Convergence	31
5.2.2	Singularities Convergence	31
5.3	Coordinate System	32
5.4	Creation of the Wake	33
5.4.1	Wake geometry	33
5.4.2	Trefftz plane coordinates	35
5.5	Paneling of the Wake	35
5.5.1	Singularity intensity in the wake	36
5.5.2	Treatment of the panels	37

5.6	Definition of the control points	42
5.7	Calculation of the Singularities Coefficients	45
5.8	Integration in Trefftz Plane	45
6	Final Results	47
6.1	Introduction to Prandtl's Theory	47
6.2	Span efficiency	49
6.3	Wing for validation	50
6.3.1	Testing the Subroutine	51
6.4	Results	51
6.5	Attempts with complex geometry	61
7	Final Comments	67
A	Description of the Subroutines	69
A.1	Subroutines Modified	69
A.2	Subroutine Created	70

List of Figures

2.1	Types of Drag	4
2.2	Finite Wing	5
2.3	Drag contributes	5
2.4	Horseshoe vortex	6
2.5	Induced Angle	6
2.6	Winglet Effects	8
2.7	Configuration	9
2.8	Non Planar Configurations	10
3.1	Potential Flow	11
3.2	Body Surface with Panel Elements	14
3.3	Panel's Influence	15
3.4	Recollocation Scheme	17
4.1	Control Volume	20
4.2	Line Integral	23
4.3	Wake's Integration	24
4.4	Trapezoidal rule 1	25
4.5	Trapezoidal rule 2	26
4.6	dl wake	26
5.1	Change in coordinate system	33
5.2	Initial Wake	35
5.3	Trefftz Plane positioning	36
5.4	Wake Paneling	36
5.5	Doublet in the Wake	37
5.6	Doublet Vortex Ring equivalence	38
5.7	Wake with Vortex Rings	38
5.8	General Vortex Panel	39
5.9	First row Vortex Panel	40
5.10	Vortex Segment	40
5.11	Tangential Velocity	42
5.12	Control Points	43
5.13	Control Points on the Nodes	44

5.14	Mid Control Points	44
6.1	Prandtl's lifting line theory	48
6.2	Flat Wake Integration	51
6.3	Core Radius	52
6.4	Radius Core Influence on the Shape a	53
6.5	Radius Core Influence on the Shape b	54
6.6	Radius Core Influence on C_{Di}	55
6.7	Offset Influence	55
6.8	Panels Influence on the Shape a	56
6.9	Panels Influence on the Shape b	57
6.10	Sections with correct C_{Di} 1	58
6.11	"Correct Shape" with no self-induction	59
6.12	Sections with correct C_{Di} 2	60
6.13	Points Integration Influence on the Shape	62
6.14	C-Wing	63
6.15	C-Wing Wake's Sections	64
6.16	Wing with Winglet	65
6.17	Wing with Winglet Wake's Sections	66
7.1	Interpenetration Problem	67

Chapter 1

Introduction

The classic finite wing theory works with a wake that lives the trailing edge in the freestream direction, and it's far away from a physical, force-free wake.

After the knowledge of the complete behaviour of the wing, the wake shape that it creates, it's also something important to define.

Since the first studies, have been seek mathematical approaches to be able to evaluate the shape, and the introduction of panel methods allowed others and better ways to define the geometry.

The wake itself influences the wing aerodynamic properties, and moreover the knowledge of the wake shape lead to a better understanding of the large scale flow behaviour; for example it's useful for formation flight in which the rear aircrafts are subjected to a perturbed flowfield generated from the aft wake.

At the Technische Universität Dresden a three-dimensional low-order panel method was developed to investigate non-planar wing configurations; this program is written with Fortran Compiler. All the information about this could be find in the reference [15].

The panel method is utilized in an aero-structural optimization framework and is therefore driven towards high computational speed.

This thesis is an improvement of the cited program that seeks to obtain the correct wake geometry and, once that this is achieved, makes the far field integration in the Trefftz plane which will be able to produce an accurate value for the wing induced drag.

Chapter 2

Info About Drag

2.1 Drag

One of the most important things in the airplane design consists in making the most efficiently flight possible; a good measure of this factor is defined by the aerodynamic efficiency, represented by the ratio lift to drag $\frac{L}{D}$.

For this reason the best way to chase it consists in minimizing the drag, but this is not as simple as it could be thought. In the study of an isolated profile the definition of lift and drag is enough simply, but when the valuation is extended on a complete wing, things start to be different and a bit complicated; the drag is made by different sources, so there are various kinds of drag like:

- airfoil profile drag
- skin-friction drag
- separation drag
- wave drag
- wave-drag-due-to-lift
- interference drag
- so forth

Figure 2.1 can make an idea of its varieties.

So many different types of drag have been defined and discussed over the years, but all of them can be gathered into the two big sources of aerodynamic forces: the pressure distribution and the shear distribution. Therefore the drag can be divided into "Pressure Drag" and "Friction Drag".

The first one is defined by the forces due to the pressure acting normal at the points on the surface; it's computed with the integral of the flight-path

		PRESSURE FORCES		
		SEPARATION	SHOCK	CIRCULATION
PARASITE DRAG	SHEAR FORCES			
	SKIN FRICTION	VISCOUS SEPARATION	WAVE DRAG	
	SCRUBBING DRAG	SHOCK-INDUCED SEPARATION "DRAG RISE"		
INDUCED DRAG [Lift]	INTERFERENCE DRAG			
	PROFILE DRAG	CAMBER DRAG		
	SUPERVELOCITY EFFECT ON SKIN FRICTION	SUPERVELOCITY EFFECT ON PROFILE DRAG - i.e., LANDING GEAR, ETC.		DRAG DUE TO LIFT TRIM DRAG
REFERENCE AREA:			WAVE DRAG DUE TO LIFT	
	S_{wet}	Max. Cross Section	(Volume Distribution)	S_{ref}

Figure 2.1: Types of Drag

component of the pressure forces.

The second instead depends directly to the viscosity, so it doesn't exist while working with hypothesis of an inviscid flow.

All the types of drag found in literature fit in one or in the other big categories described.

An important factor about drag calculation is that its analytical prediction is much harder than the lift's one.

The pressure drag can be distinct in its contributes:

- Induce drag (or "drag-due-to-lift" or "vortex drag")
- Wave drag, related to a presence of supersonic region.
- Form drag (or "boundary-layer pressure drag")

The induced drag, as the other name defined it, is strongly related to the lift produced and it's something that doesn't exist in the study of an isolated profile.

A finite wing has more drag than a profile, this is due of the wing-tip vortices that make a 3D effect; the energy needed to form those vortices in the flow field behind is taken from the wing as a drag force. The generation of the wing-tip vortices is associated with a perturbation in the pressure distribution on the wing; it produces a higher pressure over the bottom and a lower one over the top of the surfaces (see Figure 2.2)

The induced drag is the penalty paid for the lift production and it could represent the major component of the total drag, in Figure 2.3 it's shown his relevance with the others source of drag.

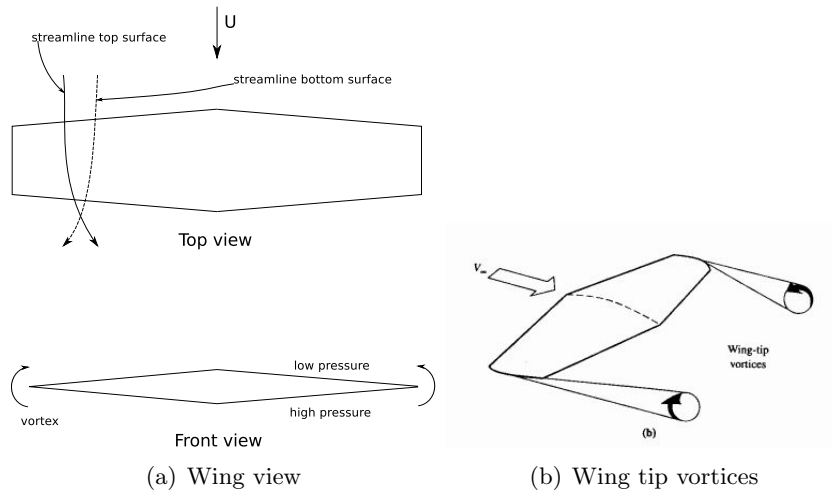


Figure 2.2: Finite Wing

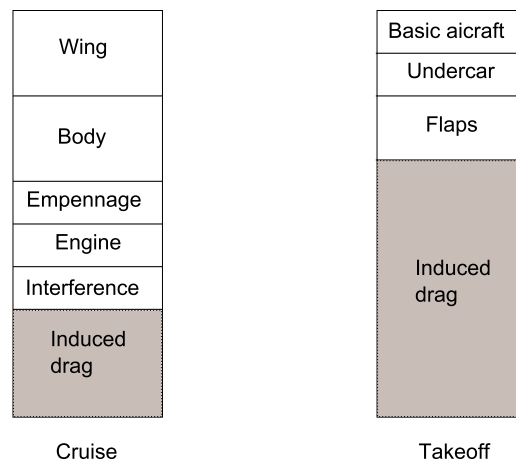


Figure 2.3: Drag contributes

It's clear how this drag could increase whenever it's required a high lift capacity.

2.2 Effects of a Finite Wing

2.2.1 Downwash

Taking as example a wing simplified with a simple horseshoe vortex system, the trailing vortex produce a downward velocity w in each span position y , called downwash or induced velocities, see Figure 2.4. This modifies the direction of the undisturbed velocity that arrives to the wing by an angle α_i called induced angle of attack, as shown in Figure 2.5.

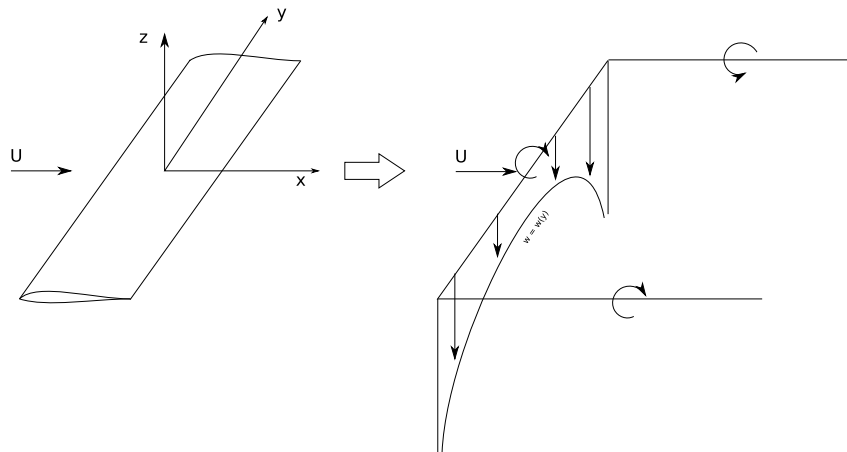


Figure 2.4: Horseshoe vortex

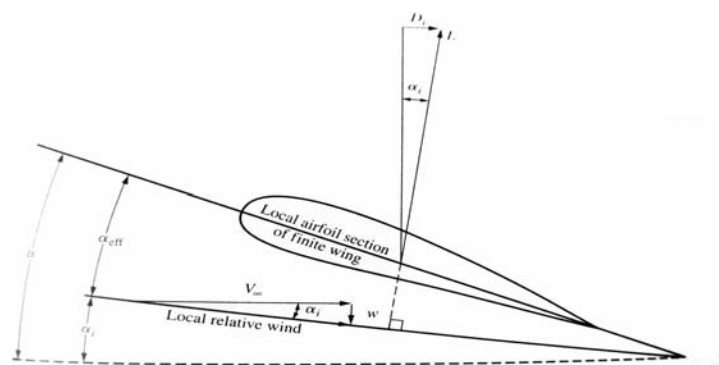


Figure 2.5: Induced Angle

Instead of coming with the geometric α_g the velocity V_∞ arrives in the local profile with the effective angle $\alpha_{eff} = \alpha_g - \alpha_i$. This effective incidence

determines the lift in the section, that is lower than the one of an isolated profile.

The circulation on the wing increases with the lift coefficient, and so the quantities w and α_i , it follows that the lift in the 3D case increases less rapidly with the angle of attack than the 2D case, due exactly for the presence of the trailing edge.

Taking the components of force generated in a section (so per unit length):

$$\begin{aligned} l &= \rho V_{eff} \Gamma \cos(\alpha_i) = \rho V_{eff} \Gamma \frac{V_\infty}{V_{eff}} = \rho V_\infty \Gamma \\ d &= \rho V_{eff} \Gamma \sin(\alpha_i) = \rho V_{eff} \Gamma \frac{w}{V_{eff}} = \rho w \Gamma \end{aligned} \quad (2.1)$$

the last is indeed the induced drag, it's evident how it's related to the downwash velocity originated by the trailing vortices.

2.2.2 Consequences of downwash

The induced velocity has two important consequences, the modification of the flow about the wing and the alteration of its aerodynamics properties.

With the simple assumption of the two-dimensional theory, taking a wing moving through air (with negligible viscosity) the static pressure of the free stream ahead is completely recovered behind the wing; this implies that all the kinetic energy produced by the wing is converted back as pressure energy, with no drag results.

But this is not the reality, till now it's like having an isolated profile or a wing with infinite span. With a real finite wing, at its extremities the unbalance in the pressure spins the airflow like in Figure 2.2(a), this makes the appearance of two trailing vortices which could have a reasonable size. Their generation needs a quantity of kinetic energy that will be not recovered by the wing system, this represents a loss of energy that the wing leaves behind. This continuous waste of energy is representative of the induced drag; related to this principle derives the equation from which this drag is calculated (see chapter 4).

From eq. (2.1) the total lift and drag become:

$$\begin{aligned} L &= \int_{-b/2}^{b/2} \rho V_\infty \Gamma dy \\ D &= \int_{-b/2}^{b/2} \rho w \Gamma dy \end{aligned} \quad (2.2)$$

an absence of induced drag will come only if the wing is working two-dimensionally or without any production of lift. The vortex system is always

produced by the basic lifting action of a real wing (with finite-span), the wing's properties are adversely modified.

From this it seems that more the wing's span is high, the more its characteristics could approach the ideal case.

2.3 Reduction of Induced Drag with Non-Planar Geometry

As said, minimizing the induced drag become an important factor in the wing design because it can become a relevant part of the total drag during the flight. For how is explained before, a solution seems to be the increase the aspect ratio of the wing, but this could be problematic for many factors like construction, dimension, weight, etc.

Instead of this, a decrease of this drag can be achieved with others kinds of expedients; one of the most used is the employment of non-planar elements like winglets, which can lead to the goal without increasing the span.

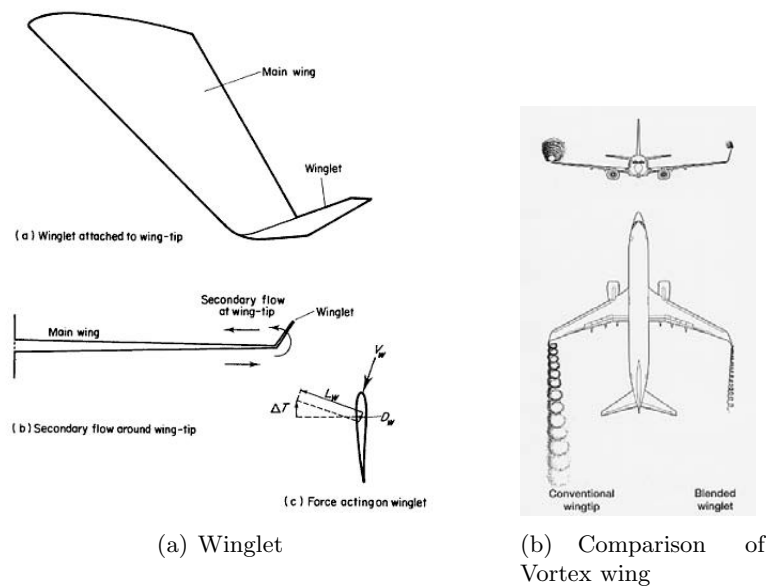


Figure 2.6: Winglet Effects

This is the first sign about how a non-planar geometry could become a way to build up airplane able to flight with a lower drag respect the standard aircraft layout. Below in Figure 2.7 it's shown an example with a wing in different C configuration with fixed span, area, and total lift.

When the lifting surface is extended till the centerline to form a box plane, is the moment in which the upper wing can efficiently carry an upload.

Therefore seems interesting the aerodynamics of non-planar wings sys-

2.3. REDUCTION OF INDUCED DRAG WITH NON-PLANAR GEOMETRY⁹

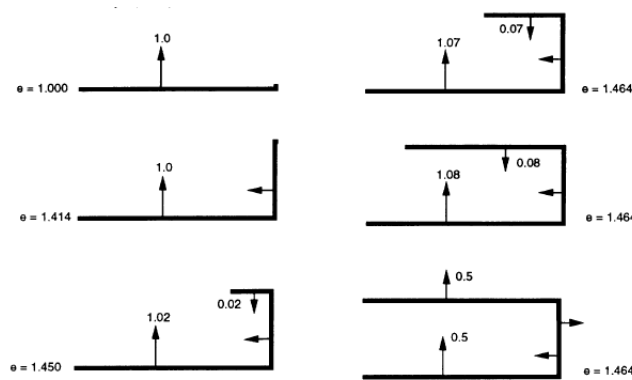


Figure 2.7: Configuration

tems that form close loops; deleting in this way the tips doesn't erase the presence of trailing vortices, but they can lower the induced drag, and apart this they can stiffen the total structure.

Those new configuration can be divided into the variants:

- Box wing: with the upper and low wings joined by vertical elements.
- Annular box wing: instead of straight components the wing tips are connected with continuous blend one.
- Cylindrical: with the wing completely shaped like a cylinder.
- Joined wings: the two are placed in different positions and one or both sweeps to join the other with a continuous surface.

Examples of those new constructions are shown in Figure 2.8

As an example (see reference [11]) the circular ring wing is subjected to an induced drag that is just 50% less than a planar wing with the same span and total lift. The Joined one achieved even a great reduction then the Cylinder, moreover the structure stiffens the structure and the wings are subjected at lower bending moments.

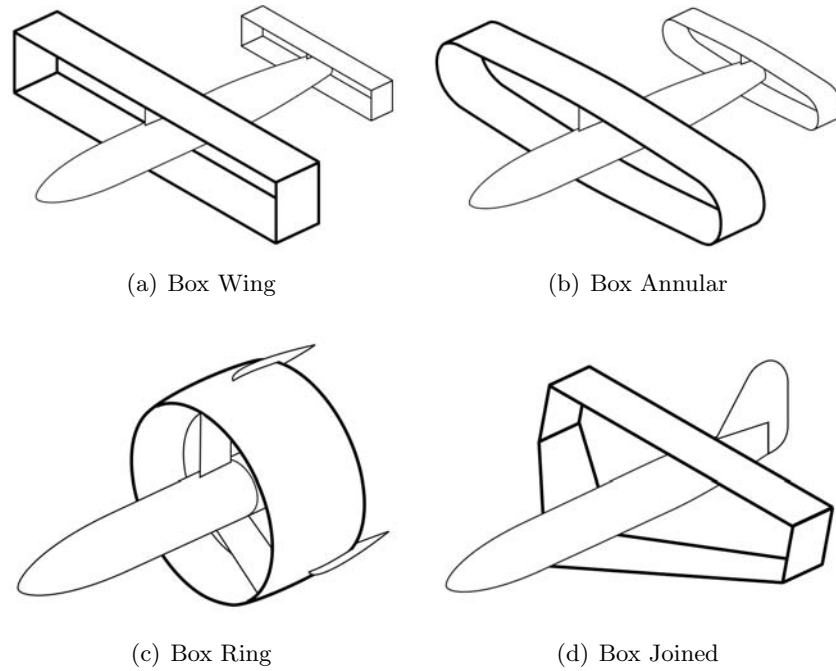


Figure 2.8: Non Planar Configurations

Chapter 3

Panel Method and Wake Relaxation

3.1 Panel Method

Here a brief explanation about the panel method; more details can be easily found in "Low Speed Aerodynamics" [9].

This is a numerical technique that allows the treatment of geometries to solve the potential flow problem and follows the hypothesis of inviscid incompressible flow.

The panel method is based on a surface distribution of source and doublet elements, and consists in finding the strength of those elements.

3.1.1 Formulation

Take in consideration a body defined by its boundaries S_B immersed in a potential flow (see Figure 3.1), in the outer region V is located the flow of interest, the irrotational equation of continuity in the body's frame in terms of total potential Φ^* is:

$$\nabla^2 \Phi^* = 0 \quad (3.1)$$

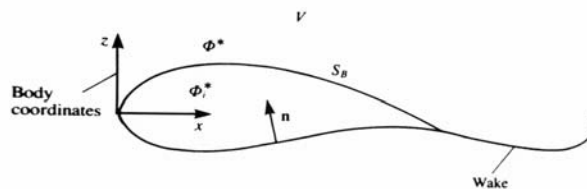


Figure 3.1: Potential Flow

The general solution of this equation is constructed like:

$$\Phi^*(x, y, z) = \frac{-1}{4\pi} \int_{S_B} \left[\sigma \left(\frac{1}{r} \right) - \mu \hat{\mathbf{n}} \cdot \nabla \left(\frac{1}{r} \right) \right] dS + \Phi_\infty \quad (3.2)$$

Where $\hat{\mathbf{n}}$ is the normal vector at the surface S_B and Φ_∞ the freestream potential defined by $\Phi_\infty = (U_{x\infty} x + U_{y\infty} y + U_{z\infty} z)$.

The source elements represent the thickness of the body and the doublet ones stand for the lifting properties.

The solution is not uniquely defined; to reach the result, boundaries condition must be applied. In three dimensional cases this is not enough to specify a solution, other decision must be defined as about the combination of source, doublet and the wake's displacement.

With a wake made by doublets the eq. (3.2) become:

$$\begin{aligned} \Phi^*(x, y, z) &= \frac{1}{4\pi} \left[\int_{body + wake} \mu \hat{\mathbf{n}} \cdot \nabla \left(\frac{1}{r} \right) dS - \int_{body} \sigma \left(\frac{1}{r} \right) dS \right] + \Phi_\infty \\ &= \Phi + \Phi_\infty \end{aligned} \quad (3.3)$$

Φ is called the perturbation potential.

3.1.2 Boundary Condition

This is done by imposing zero flow normal to the surface.

Neumann Boundary Condition

Through the Neumann condition the zero normal velocity component on S_B , defined by $\frac{\partial \Phi^*}{\partial n} = 0$, is done in a direct way:

$$\nabla (\Phi + \Phi_\infty) \cdot \hat{\mathbf{n}} = 0 \quad (3.4)$$

A second condition is imposed in the far field, where the flow disturbance due to the body diminishes:

$$\lim_{r \rightarrow \infty} \nabla \Phi = 0 \quad (3.5)$$

where $\mathbf{r} = (x, y, z)$ is the position of a point; this condition is automatically satisfied.

Using eq. (3.2) the velocities field is defined by:

$$\nabla \Phi^*(x, y, z) = \frac{1}{4\pi} \left\{ \int_{body + wake} \mu \nabla \left[\frac{\partial}{\partial n} \left(\frac{1}{r} \right) \right] dS - \int_{body} \sigma \nabla \left(\frac{1}{r} \right) dS \right\} + \Phi_\infty \quad (3.6)$$

Then the condition in eq (3.4) is rewritten:

$$\frac{1}{4\pi} \left\{ \int_{body+wake} \mu \nabla \left[\frac{\partial}{\partial n} \left(\frac{1}{r} \right) \right] dS - \int_{body} \sigma \nabla \left(\frac{1}{r} \right) dS \right\} \cdot \hat{\mathbf{n}} = 0 \quad (3.7)$$

This must be satisfied on each surfaces control points, producing in this way a system of algebraic equations.

Moreover for a closed body, nullifying the normal velocity makes the potential inside the body become $\Phi_i^* = const.$ which could be easily imposed as zero.

Dirichlet Boundary Condition

The perturbation potential Φ is specified everywhere in the body; placing a point inside it the eq. (3.3) become:

$$\Phi_i^*(x, y, z) = \frac{1}{4\pi} \left[\int_{body+wake} \mu \frac{\partial}{\partial n} \left(\frac{1}{r} \right) dS - \int_{body} \sigma \left(\frac{1}{r} \right) dS \right] + \Phi_\infty \quad (3.8)$$

the eq. (3.4) in terms of the inner potential is rewritten:

$$\begin{aligned} \Phi_i^* &= (\Phi + \Phi_\infty)_i = const. \\ &= \frac{1}{4\pi} \left[\int_{body+wake} \mu \frac{\partial}{\partial n} \left(\frac{1}{r} \right) dS - \int_{body} \sigma \left(\frac{1}{r} \right) dS \right] + \Phi_\infty = const. \end{aligned} \quad (3.9)$$

This equation makes the indirect boundary condition. A way to obtain a solution consists in specifying the inner potential as $\Phi_i^* = (\Phi + \Phi_\infty)_i = \Phi_\infty$ so:

$$\frac{1}{4\pi} \left[\int_{body+wake} \mu \frac{\partial}{\partial n} \left(\frac{1}{r} \right) dS - \int_{body} \sigma \left(\frac{1}{r} \right) dS \right] = 0 \quad (3.10)$$

This is justified by taking in consideration the Neumann condition $\frac{\partial \Phi^*}{\partial n} = 0$, that is equivalent to:

$$\frac{\partial \Phi}{\partial n} = -\hat{\mathbf{n}} \cdot \mathbf{U}_\infty \quad (3.11)$$

In the potential flow the difference between the normal derivative of external and internal potentials is:

$$-\sigma = \frac{\partial \Phi}{\partial n} - \frac{\partial \Phi_i}{\partial n}$$

so in the case studied:

$$-\sigma = \frac{\partial \Phi^*}{\partial n} - \frac{\partial \Phi_i^*}{\partial n} \quad (3.12)$$

assuming $\Phi_i^* = 0$ the source is rewritten as

$$\sigma = \hat{\mathbf{n}} \cdot \mathbf{U}_\infty \quad (3.13)$$

3.1.3 Set of Linear Algebraic Equations

With those conditions, together with a choice in which combination of source and doublet to use, the solution of the problem is assumed to be unique; the wake must be treated as well, a complete explanation of this will be found on chapter 5.5.

The system is now discretized with N panels on the body and with N_W on the wake; the boundary condition must be specified at each element in its collocation point (see Figure 3.2); the eq. (3.7) become:

$$\begin{aligned} & \sum_{k=1}^N \frac{1}{4\pi} \int_{\text{body panel}} \mu \hat{\mathbf{n}} \cdot \nabla \left(\frac{1}{r} \right) dS \\ & + \sum_{l=1}^{N_W} \frac{1}{4\pi} \int_{\text{wake panel}} \mu \hat{\mathbf{n}} \cdot \nabla \left(\frac{1}{r} \right) dS \\ & - \sum_{k=1}^N \frac{1}{4\pi} \int_{\text{body panel}} \sigma \left(\frac{1}{r} \right) dS = 0 \end{aligned} \quad (3.14)$$

For each collocation point it's the sum of the influences of all body panels k

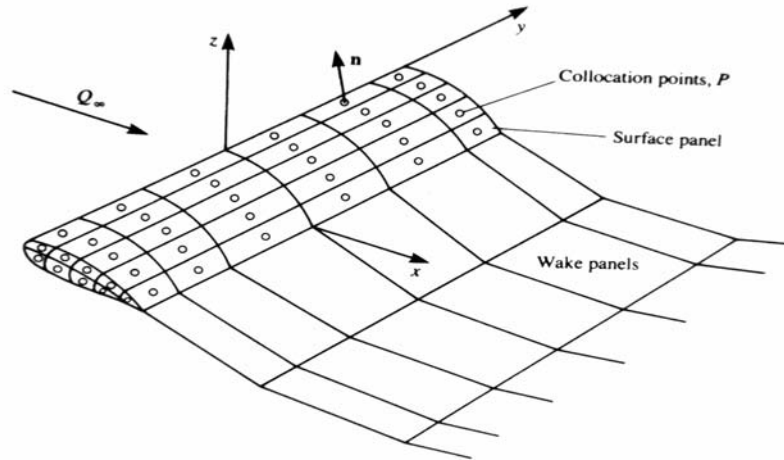


Figure 9.7 Approximation of the body surface by panel elements.

Figure 3.2: Body Surface with Panel Elements

and wake panels l ; the integration is now limited to a single panel, moreover, choosing a unity strength the influence depends solely on the geometry. Taking one wing panel the coefficients are rewritten:

$$\begin{aligned} \frac{1}{4\pi} \int_k \frac{\partial}{\partial n} \left(\frac{1}{r} \right) dS &\equiv C_k \\ \frac{-1}{4\pi} \int_k \left(\frac{1}{r} \right) dS &\equiv B_k \end{aligned} \quad (3.15)$$

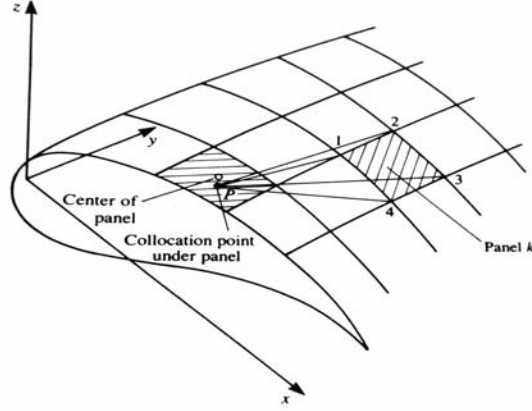


Figure 3.3: Panel's Influence

Computing the influence of all panel on each point:

$$\sum_{k=1}^N C_k \mu_k + \sum_{l=1}^{N_W} C_l \mu_l + \sum_{k=1}^N B_k \sigma_k = 0 \quad (3.16)$$

This equation is numerical equivalent to the boundary condition; furthermore though the Kutta condition the wake doublet can be expressed in terms of the wing's one. Generally the panels at the trailing edge follows $\mu_{wake} = \mu_{up} - \mu_{low}$, with arbitrary panels: $\mu_t = \mu_r - \mu_s$; in terms of the matrix it become:

$$C_t \mu_t = C_t (\mu_r - \mu_s)$$

This relation can be used to modify the doublet coefficients matrix:

$$\begin{aligned} A_k &= C_k && \text{panels not at TE} \\ A_k &= C_k \pm C_t && \text{panels at TE} \end{aligned}$$

the sing \pm depend if the panel is upper or lower at the trailing edge.

For each control points the linear algebraic equation become:

$$\sum_{k=1}^N A_k \mu_k = - \sum_{k=1}^N B_k \sigma_k \quad (3.17)$$

taking all the control points it became a matrix system:

$$\begin{pmatrix} a_{11} & a_{12} & \dots & a_{1N} \\ a_{21} & a_{22} & \dots & a_{2N} \\ \dots & \dots & \dots & \dots \\ a_{N1} & a_{N2} & \dots & a_{NN} \end{pmatrix} \begin{pmatrix} \mu_1 \\ \mu_2 \\ \dots \\ \mu_N \end{pmatrix} = - \begin{pmatrix} b_{11} & b_{12} & \dots & b_{1N} \\ b_{21} & a_{22} & \dots & b_{2N} \\ \dots & \dots & \dots & \dots \\ b_{N1} & b_{N2} & \dots & b_{NN} \end{pmatrix} \begin{pmatrix} \sigma_1 \\ \sigma_2 \\ \dots \\ \sigma_N \end{pmatrix} \quad (3.18)$$

With the values of sources evaluated by eq. (3.13) the eq. (3.18) are rewritten:

$$\begin{pmatrix} a_{11} & a_{12} & \dots & a_{1N} \\ a_{21} & a_{22} & \dots & a_{2N} \\ \dots & \dots & \dots & \dots \\ a_{N1} & a_{N2} & \dots & a_{NN} \end{pmatrix} \begin{pmatrix} \mu_1 \\ \mu_2 \\ \dots \\ \mu_N \end{pmatrix} = \begin{pmatrix} RHS_1 \\ RHS_2 \\ \dots \\ RHS_N \end{pmatrix} \quad (3.19)$$

Then doublet values μ_i are computed solving the matrix equation.

3.2 Relaxation Process

Till the firsts years of the aerodynamic studies, ways to define the wake's shape have been sought; with simple wing even applying a mathematical method that predict the evolution of the vortex flow behind the wing.

With the application of the panel method more improvement was achieved.

The true shape can be reached with two different methods:

- spatial-relaxation;
- time-stepping.

The first starts with an hypothetical wake shape from which begin to reallocate its nodes with an iterative process.

The time-stepping instead considers a wing moving forwards at a constant velocity U_∞ and with it, repositioning the wake that evolves at each time step.

Searching information about the difference between this two, the only thing found is that the second is more suitable for the study of unsteady motion, but information about difference like speed of convergence, reliability or other of the two methods haven't been found.

The process takes advantage of the panel method application; the most recent applications use high order elements capable of a better representation of the system wing, coupled with this comes the wake schematization.

Some article in the "American Institute of Aeronautics and Astronautics Journal (AIAA)" have a brief description about the treatment of the wake and the methods to reach its roll-up (see [6], [14], [13], [4], [7]).

To achieve the best shape approximation in those reports are applied different methods.

One way described in [6] use a wake made by a vortex sheet, and at fixed time steps employs an adaptive curvature paneling scheme to evaluate the geometry in a section, this is said that can provide a good definition of the nodes.

The others use panel elements with a distributed vorticity or curved panel, so high order elements.

Those articles are not so strictly helpful for our purpose, but they have useful hints that can be applied.

3.2.1 Points Evaluation

The theory behind the process is rather simple, being the wake tangential to the flowfield all the vortex line of the sheet are stream line and they must satisfy their equation:

$$\frac{dy}{dx} = \frac{v + U_y}{u + U_x} \quad \frac{dz}{dx} = \frac{w + U_z}{u + U_x} \quad (3.20)$$

where the $[U_x U_y U_z]$ are the components of the stream velocity U_∞ and $[u v w]$ those of the induced velocity in a generic system of reference.

The spatial-relaxation process becomes an iterative procedure in which, taking a point in the wake, the next one in the freestream direction (x -coordinate) is evaluated by the integration of the eq. (3.20).

From each step the displacement are shed downstream to adapt the entire wake like in Figure 3.4.

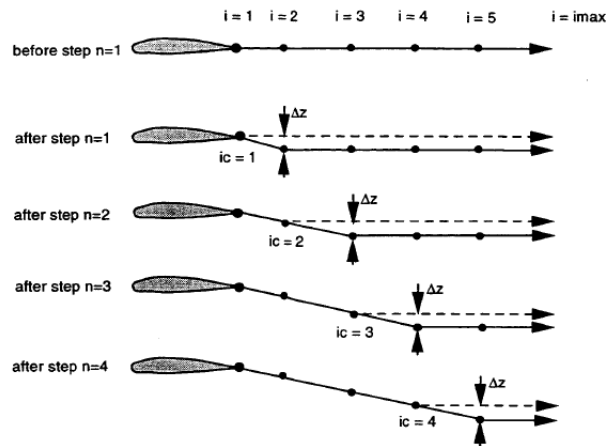


Figure 3.4: Relocation Scheme

Chapter 4

Induced Drag Calculation

The induced drag can be calculated by a pressure integration on the wing surface, but in this way the results obtained are not enough accurate for a well examination of the wing behaviour.

This kind of problem with the integration is due of the fact that for some wing configuration the computation of the integration involves subtractive cancellation, this causes a loss of accuracy when computing small variation of small quantity.

An alternative way consists in the far-field method, evaluating the drag through the *Trefftz plane*.

4.1 Equation development

As noted in section 2.2.2 an expression for the induced drag can be obtained from the momentum conservation.

Von Karman said that by surrounding a wing with a control volume, the conservation principles could be applied for the induced drag calculation.

For the derivation of the equation it's taken the control volume in Figure 4.1 fixed in the inertial reference frame of the wing and moving with the constant velocity U_∞ of the undisturbed flow. Without any external forces, the conservation of momentum in the volume is given by:

$$\mathbf{F} = \frac{D\mathbf{P}}{Dt} = -\frac{d}{dt} \iiint \rho \mathbf{V} dv - \iint \rho \mathbf{V} (\mathbf{V} \cdot \hat{\mathbf{n}}) ds = 0 \quad (4.1)$$

With the hypothesis of inviscid and steady-state flow the equation become:

$$\iint p \hat{\mathbf{n}} ds = - \iint \rho \mathbf{V} (\mathbf{V} \cdot \hat{\mathbf{n}}) ds \quad (4.2)$$

The purpose of this project is the study of the drag, so only the component on x direction is necessary for the equation; in this way:

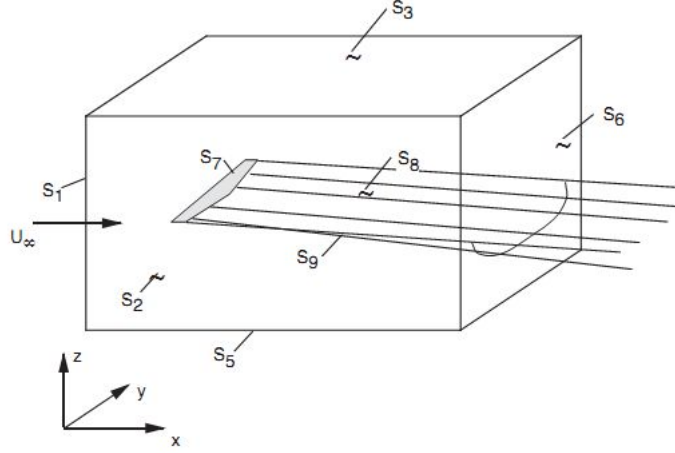


Figure 4.1: Control Volume

$$\iint pn_x ds = - \iint \rho V_x (\mathbf{V} \cdot \hat{\mathbf{n}}) ds \quad (4.3)$$

This is for all the surfaces of the control volume; now the contribution of each integral is evaluated individually.

S_8 & S_9

For a force-free wake aligned everywhere with the local flow there is no pressure difference and the scalar product $(\mathbf{V} \cdot \hat{\mathbf{n}})$ is zero on the wake surfaces so:

$$\begin{aligned} \iint_{S_8} pn_x ds + \iint_{S_9} pn_x ds &= 0 \\ \iint_{S_8, S_9} \rho V_x (\mathbf{V} \cdot \hat{\mathbf{n}}) ds &= 0 \end{aligned} \quad (4.4)$$

S_7

This is the one that surrounds the wing, in this surface it's true that $(\mathbf{V} \cdot \hat{\mathbf{n}}) = 0$ and the pressure integrals:

$$\iint_{S_7} pn_x ds = D \quad (4.5)$$

For an inviscid and subsonic flow this drag represents the induced drag D_i .

The remaining component

The others surfaces are the ones of the volume, and the normal takes values: for S_3, S_5, S_2 and S_4 $n_x = 0$, on S_1 $n_x = -1$ and on S_6 it's $n_x = 1$. For the next steps it's useful make in evidence the perturbation components from the freestream ones; respectively (u, v, w) and U_∞ for the velocities and p, p_∞ for the pressures. The complete expression of the eq. (4.3) become:

$$\begin{aligned}
D_i + \iint_{S_6} (p - p_\infty) ds - \iint_{S_1} (p - p_\infty) ds = \\
- \iint_{S_3} \rho(U_\infty + u)w ds + \iint_{S_5} \rho(U_\infty + u)w ds + \\
+ \iint_{S_2} \rho(U_\infty + u)v ds - \iint_{S_4} \rho(U_\infty + u)v ds + \\
+ \iint_{S_1} \rho(U_\infty + u)^2 ds - \iint_{S_6} \rho(U_\infty + u)^2 ds
\end{aligned} \tag{4.6}$$

For a stationary flow, the mass conservation through the volume is defined from:

$$\iint \rho(\mathbf{V} \cdot \hat{\mathbf{n}}) ds = 0 \tag{4.7}$$

in terms of the perturbation velocities:

$$\begin{aligned}
\iint_{S_3} \rho w ds - \iint_{S_5} \rho w ds - \iint_{S_2} \rho v ds + \iint_{S_4} \rho v ds + \\
- \iint_{S_1} \rho(U_\infty + u) ds + \iint_{S_6} \rho(U_\infty + u) ds = 0
\end{aligned} \tag{4.8}$$

inserting this on the eq. (4.6) yields:

$$\begin{aligned}
D_i + \iint_{S_6} (p - p_\infty) ds - \iint_{S_1} (p - p_\infty) ds = \\
- \iint_{S_3} \rho u w ds + \iint_{S_5} \rho u w ds + \iint_{S_2} \rho u v ds - \iint_{S_4} \rho u v ds + \\
+ \iint_{S_1} \rho u(U_\infty + u) ds - \iint_{S_6} \rho u(U_\infty + u) ds
\end{aligned} \tag{4.9}$$

When the size of the control volume is increased the contribute of the surfaces from 1 to 5 becomes very small, and neglecting those terms the equation change into:

$$D_i = - \iint_{S_6} (p - p_\infty) ds - \iint_{S_6} \rho u(U_\infty + u) ds \tag{4.10}$$

The next step consists in finding a relationship between the pressure and the velocity on S_6 , this is done using the Bernoulli's equation.

For any subsonic freestream, assuming small perturbation and isentropic flow, a second-order form of the equation is defined by:

$$p - p_\infty = \frac{1}{2}\rho_\infty \left(2uU_\infty + (1 - M_\infty^2)u^2 + v^2 + w^2 \right) \quad (4.11)$$

Inserting this in the eq. (4.10) results:

$$\begin{aligned} D_i &= \frac{1}{2}\rho_\infty \iint_{S_6} \left(2uU_\infty + (1 - M_\infty^2)u^2 + v^2 + w^2 \right) ds - \iint_{S_6} \rho u(U_\infty + u) ds \\ &= \frac{1}{2}\rho_\infty \iint_{S_6} \left(2uU_\infty - M_\infty^2 u^2 + (u^2 + v^2 + w^2) \right) ds - \iint_{S_6} \rho u(U_\infty + u) ds \end{aligned} \quad (4.12)$$

This become:

$$D_i = \frac{1}{2}\rho_\infty \iint ((M_\infty^2 - 1)u^2 + v^2 + w^2) ds \quad (4.13)$$

neglecting the Mach number:

$$D_i = \frac{1}{2}\rho_\infty \iint (-u^2 + v^2 + w^2) ds \quad (4.14)$$

Also the wake is parallel to the freestream and it can be assume that $u^2 \ll v^2 + w^2$; the u -component can be ignored.

The flow is a potential flow, so the velocities could be written with it in this way:

$$\begin{aligned} \iint (u^2 + v^2 + w^2) ds &= \iint \left\{ \left(\frac{\partial \phi}{\partial x} \right)^2 + \left(\frac{\partial \phi}{\partial y} \right)^2 + \left(\frac{\partial \phi}{\partial z} \right)^2 \right\} ds \\ &= \iint \nabla \phi \cdot \nabla \phi ds \end{aligned} \quad (4.15)$$

It holds that $\nabla \phi \cdot \nabla \phi = \nabla \cdot \phi \nabla \phi - \phi \nabla^2 \phi$, in addition $\nabla^2 \phi = 0$ outside the wake, so :

$$\iint (u^2 + v^2 + w^2) ds = \iint \nabla \cdot \phi \nabla \phi ds \quad (4.16)$$

separating the components into the cross flow and the freestream:

$$\begin{aligned} \iint \nabla \cdot \phi \nabla \phi ds &= \iint \left\{ (\nabla \cdot \phi \nabla \phi)_{xy} + \frac{\partial}{\partial x} \left(\phi \frac{\partial \phi}{\partial x} \right) \right\} ds \\ &= \iint \left\{ (\nabla \cdot \phi \nabla \phi)_{xy} + \phi \frac{\partial u}{\partial x} + u^2 \right\} ds \end{aligned}$$

Using the Gauss' theorem it's possible relates the surface integral into a line integral following its rule: $\iint \nabla \cdot \mathbf{a} ds = \oint \mathbf{a} \cdot \hat{\mathbf{n}} dl$ so:

$$\iint \nabla \cdot \phi \nabla \phi ds = \oint \phi (\nabla \phi \cdot \hat{\mathbf{n}}) dl = \oint \phi \left(\frac{\partial \phi}{\partial n} \right) dl \quad (4.17)$$

Furthermore if the control volume is large enough the perturbation velocities will vanish everywhere except on the wake, so in the eq. (4.12) will remain only the element linked to the line integral on the surface S_6 :

$$D_i = \frac{1}{2} \rho_\infty \oint \phi \left(\frac{\partial \phi}{\partial n} \right) dl \quad (4.18)$$

The path of the integration follows what is shown in Figure 4.2:

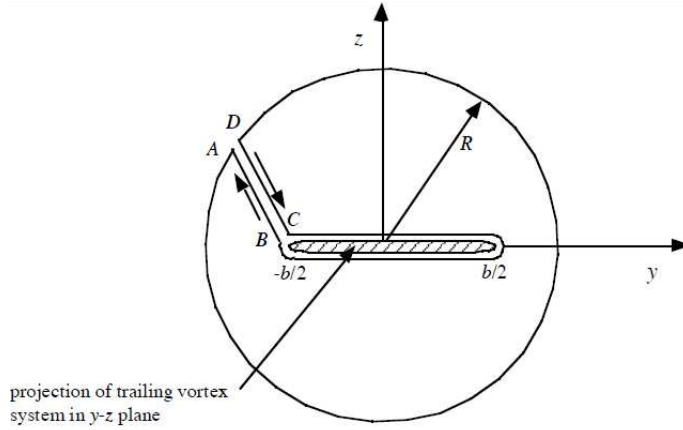


Figure 4.2: Line Integral

Given that the volume is big enough the contribute on line A-D vanishes, also the integrals along A-B and C-D cancel each other; therefore only the contribution of the path that contains the wake will gain a value to the integration. In addition of this, the potential ϕ on the wake is equal to the jump of potential shed from the wing at the trailing edge $(\nabla \phi)_{TE}$, and the $\frac{\partial \phi}{\partial n}$ it's nothing else but the downwash velocity w .

The eq. (4.18) could be rewritten as:

$$D_i = \frac{1}{2} \rho_\infty \int_{wake} (\nabla \phi)_{TE} w dl \quad (4.19)$$

This is the final equation that will be used to evaluate the induced drag.

The coefficient of the induce drag is calculated with the standard formula:

$$C_{Di} = \frac{D_i}{q_\infty S_{ref}} \quad (4.20)$$

where $q_\infty = \frac{1}{2}\rho_\infty V_\infty^2$ is the dynamic pressure and S_{ref} the reference area of the wing, it could be the plan area or the wetted area, depends on the choices made.

Calling the integral $\int_{wake} (\nabla\phi)_{TEW} dl = I_{Di}$ and substituting eq. (4.19) into the (4.20) the induce drag coefficient becomes now:

$$\begin{aligned} C_{Di} &= \frac{\frac{1}{2}\rho_\infty I_{Di}}{\frac{1}{2}\rho_\infty V_\infty^2 S_{ref}} \\ &= \frac{I_{Di}}{V_\infty^2 S_{ref}} \end{aligned} \quad (4.21)$$

4.2 Integration of the Induced Drag

Obtained the right equation, the next step consists in producing the numerical integration. Here enter the relaxation process with which the shape on the wake will be defined.

The condition of infinity of the position for the Trefftz plane is obviously impossible, it is shown in reference [17] that the plane must be far enough downstream of the lifting system to make valid the assumption in eq. (4.19); placing it at approximately 15 or 16 semispans from the wing is the common choice made in all the reports found; also to take count of a representative infinite wake the remain of it is extended till 30 semispans.

As will be explained in chapter 5.4 the section of the Trefftz plane is defined from the wake's creation.

Following the advise in [17] in order to evaluate the wake's properties a couple of survey points are placed above and below the wake as exposed in Figure 4.3. This is done using the midpoints of the panels and constructing

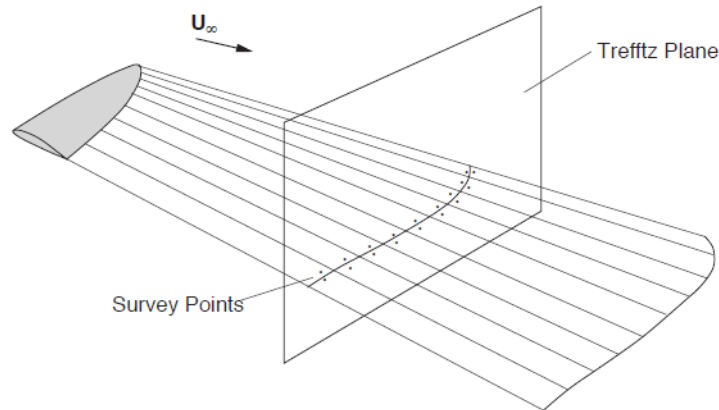


Figure 4.3: Wake's Integration

the control points from them (like what explained in the chapter 5.6).

The velocity in a station point will be the average of the two control points.

The final step consists in applying a numerical method to solve the integral (4.19); the best choice should be use the trapezoidal rule.

Trapezoidal Rule of Integration

For a generic function $f(x)$ defined in the extremes a and b (Figure 4.4) the integration is defined:

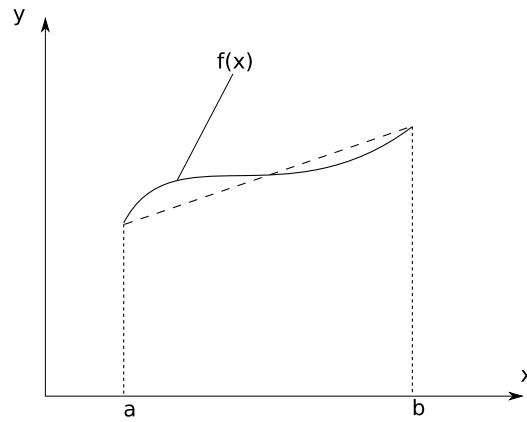


Figure 4.4: Trapezoidal rule 1

$$\int_a^b f(x) dx = (b - a) \left(\frac{f(a) + f(b)}{2} \right) \quad (4.22)$$

for a better estimation the length of integration can be divided in elements:

$$\int_a^b f(x) dx = \sum \Delta x_n \left(\frac{f(x_i) + f(x_{i+1})}{2} \right) \quad (4.23)$$

Application on the Wake

For the evaluation of the induced drag the integral becomes:

$$I = \sum dl \left(\frac{\mu_a w_a + \mu_b w_b}{2} \right) \quad (4.24)$$

Where dl is the distance from two point, w the velocity and μ the doublet intensity shed from the trailing edge of the wing.

Furthermore the elements dl are the distance between the two midpoints; they are evaluated through a fictitious curvilinear coordinate that follows the shape of the wake like Figure 4.6

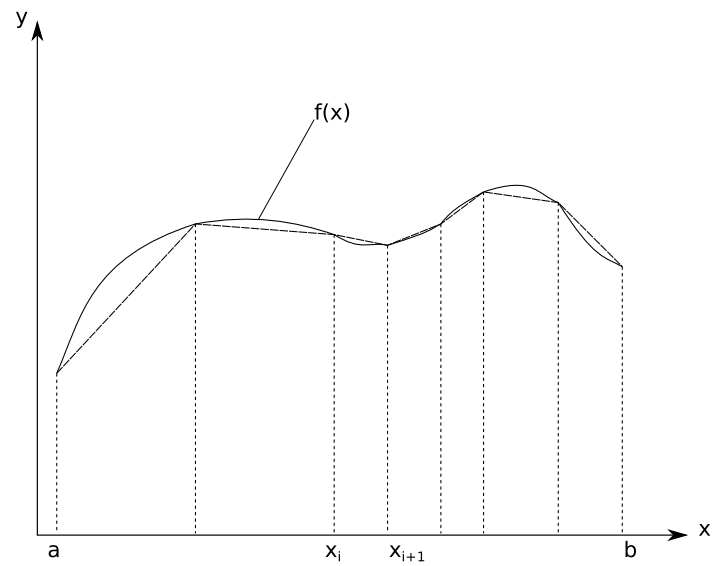


Figure 4.5: Trapezoidal rule 2

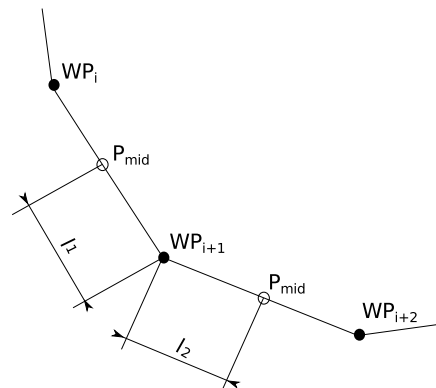


Figure 4.6: dl wake

With the geometry known it's an easy task; the midpoints are simply calculated with the wake's points, then the distance between them is defined through $dl = l_1 + l_2$.

Chapter 5

Description of the program

The basic program written by Dipl.-Ing. Uwe Schuster applies a low order panel method to the study of a wing with an arbitrary geometry, evaluating its aerodynamic properties.

The surface is simplified by a distribution of source and doublet made by constant strength. The hypothesis of work are based on an inviscid, incompressible fluid in a steady state. A complete description of the program can be found in reference [15].

What will be here explained is an improvement of this program with the purpose of evaluating the real wake shape.

5.1 Iteration Process

The relaxation process follows those steps:

1. create the control points on the first wake rows of nodes
2. evaluate the velocity in those points induced by:
 - the wing
 - the entire wake
 - the velocity of the flow U_∞
3. define the velocity at each node from the average of the one on the control points
4. displace the next nodes tangent to the velocities
5. repositioning all the downstream nodes
6. define the new distribution of singularities
7. start again from the next row of nodes

5.1.1 Points Integration

The points of the wake must satisfy the condition of the streamlines:

$$\frac{dy}{dx} = \frac{v + U_y}{u + U_x} \quad \frac{dz}{dx} = \frac{w + U_z}{u + U_x}$$

To achieve a solution those equation must be integrated through a numerical method; the most used is the Euler method because is rather simple and required not much calculation. Another one here applied follows the trapezoidal scheme, it's a 2 step method; the stability and reliability are higher than the Euler one, but required the double of the computational burden.

Calling $f(x, y)$ e $f(x, z)$ the functions with the velocities, the evaluation of the next point with the Euler way become:

$$y_{i+1} = y_i + f(x, y)\Delta x \quad z_{i+1} = z_i + f(x, z)\Delta x \quad (5.1)$$

Instead through the 2-step for the z component:

$$\begin{aligned} \bar{z}_{i+1} &= z_i + f(x, z)\Delta x \\ z_{i+1} &= z_i + \frac{\Delta x}{2} (f(x, z) + f(x_{i+1}, \bar{z}_{i+1})) \end{aligned} \quad (5.2)$$

the length Δx is the distance in x-coordinate from the point in analysis and the next one.

With complex geometry or to avoid any risk of divergence with the development of the iterations, it's introduced an under-relaxation factor f , a correction value that lightens the updated solution reducing any error that could occur with the process. Following this idea the next point's position is corrected like:

$$\begin{aligned} dy &= f(y_{i+1}^* - y_{i+1}^{n-1}) \\ dz &= f(z_{i+1}^* - z_{i+1}^{n-1}) \end{aligned} \quad (5.3)$$

Where y_{i+1}^* and z_{i+1}^* are the points evaluated from the (5.1) or (5.2); y_{i+1}^{n-1} and z_{i+1}^{n-1} are instead the position of the nodes in the previously iteration; as cited in [17] using a value of $f = 0.5$ is suitable for the solution (for simple geometry $f = 1$ works well).

5.2 Seeking convergence

In the process there are two big variables that continue changing.

The wake shape is modified at each step and due to the new geometry configuration the distribution of singularities is modified too.

Starting from this configuration the initial singularities are evaluated.

5.2.1 Geometry Convergence

While the process continuous the reposition of the wake, a criterion to stop it it's necessary. The simplest way consists in defining a tolerance, checking it after each complete movement. The value selected is $0.001 b/2$, proportional to the wing span.

Then after each nodal displacement the program checks both the Δz and Δy movements finding the maximum one and saving it in a vector; after a complete iteration the biggest displacement is found again in this vector. When this maximum value remains under the tolerance for three complete iteration the wake is considered converged to its finally shape and the iteration stops.

5.2.2 Singularities Convergence

Once again, the wake is in a constant geometric change, this is a thing that affects the doublet distribution on the wing, and then the μ on the wake itself. So the proper way to approach this problem should be calculates again the influence coefficients C_V_Strip and the singularities after each movement of row but, because of the high number of panels in the system wake-wing, doing this takes a lot of computational time, so a way to save it may be plays with the recalculation.

Moreover during the firsts iterations the wake is subjected whit the biggest displacements, so it's supposed that here the relevance of the doublet distribution should be much more influential, and due to this it's setted that in those steps the recalculation of the influence coefficients and of course the singularities will happen more frequently. With the progress of the iterations the gap between one recalculation and the next will increase following what are explained in the table (5.1):

iteration n^{th}	recalc step
1 - 5	5
6 - 10	10
11 - ...	20

Table 5.1: Singularity recalculation

There will be a moment in which the changing of the singularities will be irrelevant for the calculation, so a check on the convergence of those is inserted.

After each complete wake movement the doublets that are shed from the wing are calculated and compared with the ones of the previously iteration; if the maximum value of those $(\Delta\mu)_{TE}$ is less than the chosen tolerance ***mu.toll*** the doublets are considered converged and from the next cycle the influence coefficients and the singularities will be evaluated only after a

complete movement. This only to not let any little influence of change to get lost from one iteration to the next.

For this purpose the logical variable *mu_recalc* is inserted; from the beginning it's setted up *.true.* and when the convergence is reached it will be imposed as *.false.* erasing the recalculation process.

Furthermore, exist cases like wings with large aspect ratio, in which the effect of the wake roll-up on the wing loading is negligible (found by Suci and Morino [5]) so there's no need of the recalculation of the singularities and this procedure could be stopped since the beginning with the logical variable.

So the relevance of the singularities redefinition depends on the wing shape besides the wake geometry.

5.3 Coordinate System

The derivation of the drag formula explained in Chapter 4 is made in a coordinate system that has the x -coordinate parallel to the U_∞ direction; the Trefftz plane is also orthogonal to it.

So it have been chosen to change the default frame of reference and start working on this.

With the hypothesis that the velocity comes with no other inclination that the standard angle of attack α , the new system (VCS) can be obtained with a simple rotation in the y -coordinates; taking a generic angle θ the change of frame is obtained with the matrix:

$$[R_{(\theta)}] = \begin{bmatrix} \cos \theta & 0 & -\sin \theta \\ 0 & 1 & 0 \\ \sin \theta & 0 & \cos \theta \end{bmatrix}$$

In our case the rotation is done with the angle $\theta = -\alpha$ like in Figure 5.1, so taking a generic point $P(x_P, y_P, z_P)$, its coordinates in the new frame are rewritten:

$$\begin{pmatrix} x_{P\infty} \\ y_{P\infty} \\ z_{P\infty} \end{pmatrix} = [R_{(-\alpha)}] \begin{pmatrix} x_P \\ y_P \\ z_P \end{pmatrix}$$

To start working with this new frame the conversion is applied to the vector *AdvWingPoints*; with the wing points written here all the others variables in the program will follow this frame (the wake too is build from those points, this will be explained in 5.4.1).

Important fact

Now that the coordinate system is changed, particular attention must be taken in the calculations, precisely where there's the need of the angle of

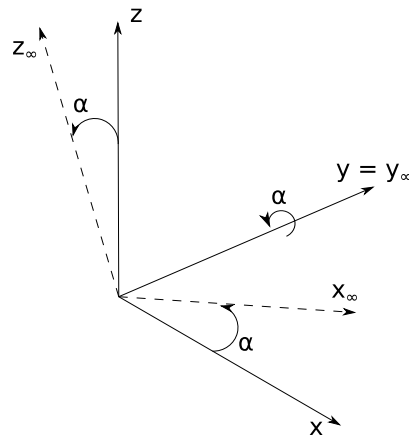


Figure 5.1: Change in coordinate system

attack like the subroutines *PanelStrengths*, *AeroCoeff* and *Evaluation*, and when the unitary undisturbed velocity U_∞ (called **OnsetFlow**) is defined. For how the calculation are build, now it must be set $\alpha = 0^\circ$ because the flows direction is now the same as the x -coordinate.

5.4 Creation of the Wake

5.4.1 Wake geometry

The points that define the wake are build up starting from the wing ones, those are now written in the stream coordinate system so the new points will be related to it too.

Searching in literature, something useful have been found about how create the wake; in the article in reference [2] is explained how its length can be separated in different regions:

- Adjoin zone;
- Near Field;
- Far Field.

The first region in the one attached to the trailing edge and it's made with shorter panels; this due to the fact that any kind of error on the shape in the proximity of the trailing edge will be propagated to the downstream compromising the results of the analysis.

The most important fact about this zone regards the first row of panels, because its meaning consists in the satisfaction of the Kutta condition: the velocity that exits from the profile trailing edge must be tangent to it. So the first row of points that originate the panels are build in the direction of the local bisector of each profile end (see Figure 5.2), and it won't be moved

during the iteration process; this is enough to guarantee it.

This row is made smaller than the others in the adjoin region, it's set to be $0.05 b/2$.

The Near Field is the region where the wake starts to roll-up itself, and it's said that it extends itself till 6 semispans from the trailing edge.

Here the panels have a higher density, meaning that there are more rows in the streamwise direction, again like the Adjoin region this is done because any kind of errors in the shape will be propagated downstream.

In the Far Field the Trefftz Plane takes place, and for this reason it has been chosen to divide this region into two, the first called Far Field 1 till the plane position and the second, Far Field 2, till the end of the wake. The motivations of this are based on the wake section; the numerical integration of the induced drag (eq. (4.24)) is highly sensitive to the wake shape obtained, so the introduction of the first region seems a reasonable solution to gain a better control on the geometry.

Discretization of the Wake

The free variables for the wake's discretization are the length of the fields and the number of panels to use in each of the regions described before:

- *WakeLength*;
- *NearField*;
- *TP_Position*;
- *NPAdjoin*;
- *NPNearField*;
- *NPFarField_1*, *NPFarField_2*.

The first three define the wake region dimensions, the last two their paneling.

WakeLength is the complete length of the wake and it's inserted in the input file, most of the studies put it equal to $30b/2$, a reasonable length that simulates an infinite wake; the second sets the extension of the Near Field; *TP_Position* is the one that imposes where the Trefftz plane is placed, commonly at $16 b/2$.

In the Adjoin zone, the total length depends on the number of panels selected (*NPAdjoin*); the first row, as explained, is fixed, for the others it's chosen to set the panel length equal to $0.05 b/2$.

The other variables define the number of panels from which to discretize the related regions.

The wake created in this way is also the one that represents the initial geometry for the iteration, and represents itself a crucial factor; this initial shape could facilitate the process or not. In reference [17] it's said that a

suitable first wake is placed with an angle of inclination equal to $\alpha/2$ like in Figure 5.2.

So the first row is the only one placed following the bisector, and from the second the inclination of the downstream points follows the addition of this angle.

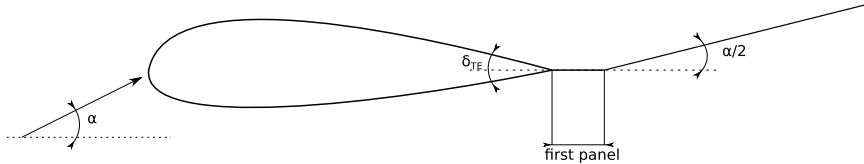


Figure 5.2: Initial Wake

5.4.2 Trefftz plane coordinates

The purpose of this project is the integration on the Trefftz plane after the relaxation process; as explained in chapter 4 the intersection with the wake here will individuate the points to be studied.

So one problem consists on a method to define this section in a simple way.

As explained till now the wake points displacement depends on the geometry of the wing, more precisely from the trailing edge ones, the position from which they are shed; for example with a swept wing the wake points in the same row will have different x -coordinates, and individuate the position (x_{TP}, y_{TP}, z_{TP}) of the necessary wake points could become complicated. The solution chosen consists in the creation of those points ad hoc.

First of all the wing's trailing edge points are scanned to find the most backward one and from it's calculated the x -coordinate where place the plane. Then the program goes on normally till the second to last row of nodes in the Far Field 1 and the next one is placed with all its nodes at the same x -coordinate x_{TP} ; from this the right displacements Δy and Δz are evaluated to continue the correct points placement in y_{TP} and z_{TP} .

Furthermore their position *ii*. TP in the vector **WakePoints** is saved, so the cross-section will be easily found when it will be needed. After this the wake creation goes on creating the remains points in the Far Field 2.

5.5 Paneling of the Wake

Once the geometry is created the next step consist in adapting it for the panel treatment.

All the nodes are gathered into quadrilateral panels, those are numbered following on strip at a time, from the begin to the end of it like in Figure 5.4.

The panels count continues from the wing ones. For each of them all the geometric properties are defined: corner points, local coordinate system, the

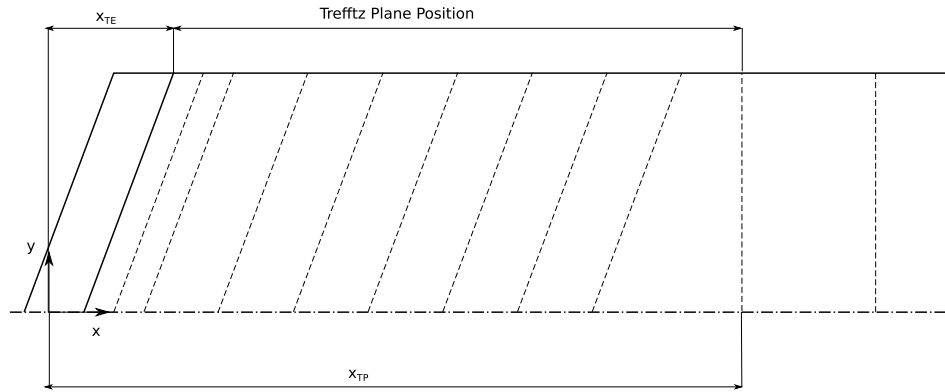


Figure 5.3: Trefftz Plane positioning

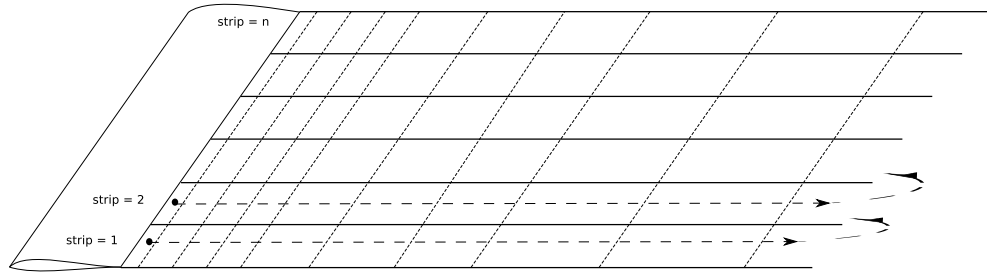


Figure 5.4: Wake Paneling

rotational matrix and corner points in the local coordinates.

5.5.1 Singularity intensity in the wake

With the panel methods the panels in the wake are defined through doublets, the intensities imposed are related to the wing singularities distribution.

As explained in "Low Speed Aerodynamics" [9], from the Kutta condition in the wake is shed a singularity μ of constant intensity equal to the value assumed at the trailing edge; taking a strip of the wing and making particular attention on the two panels that form the end of the wing (see what is shown in Figure 5.5) the panel ends up to have a strength of:

$$\mu_{up} - \mu_{low} - \mu_{wake} = 0 \quad (5.4)$$

that leads obviously at:

$$\mu_{wake} = \mu_{up} - \mu_{low} \quad (5.5)$$

Moreover the wake will not produce any lift, writing the Kutta-Joukowski theorem it holds:

$$\Delta \mathbf{F} = \rho \mathbf{V} \times \gamma = 0 \quad (5.6)$$

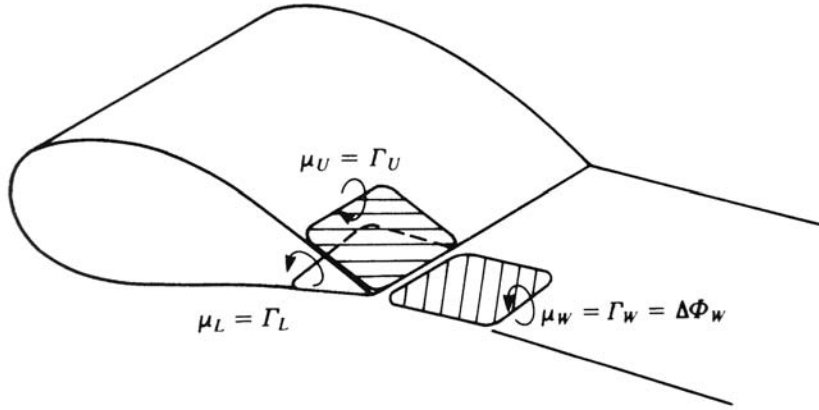


Figure 5.5: Doublet in the Wake

with \mathbf{V} the local velocity and γ the vortex intensity; this formula is equal to 0 only when the vectors are parallel. An equivalent representation of the wake with doublet is achieved with $\gamma_{wake} = -\Delta\mu_{wake}$, the eq. (5.6) become:

$$\mathbf{V} \times \Delta\mu_{wake} = 0 \quad (5.7)$$

then the condition for the wake panels is:

$$\mu_{wake} = constant \quad (5.8)$$

5.5.2 Treatment of the panels

The wake is then represented with a sheet of doublet panels and it have been suggested to take advantage of the doublet - vortex ring equivalence with: $\Gamma = \mu$ as described again in [9].

So each side of the ring will now be treated like a single and simple vortex segment; and in this way the schematization for the calculation become something like Figure 5.7.

With this new configuration some more observation can be made in order to save computational time.

Vortex Ring

In a same strip with the same doublet intensity all the adjacent panel elements will erase their effect one another during a normal calculation; this is done as note in the Figure 5.7, all those elements have the same Γ_i but with opposite signs.

In order to avoid useless calculation and in this way save time, the standard treatment of the rings is modified.

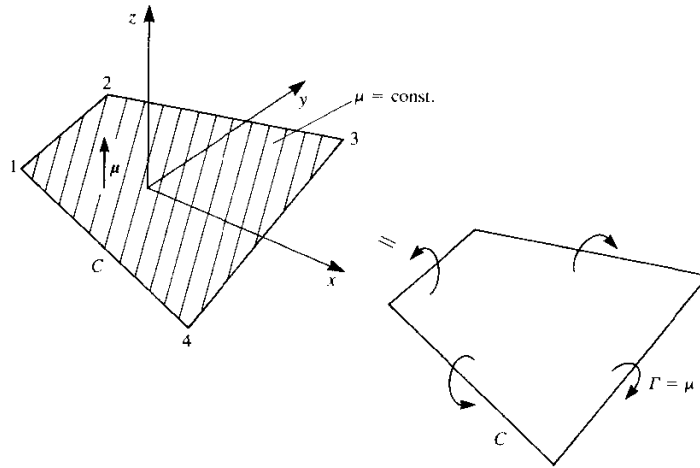


Figure 5.6: Doublet Vortex Ring equivalence

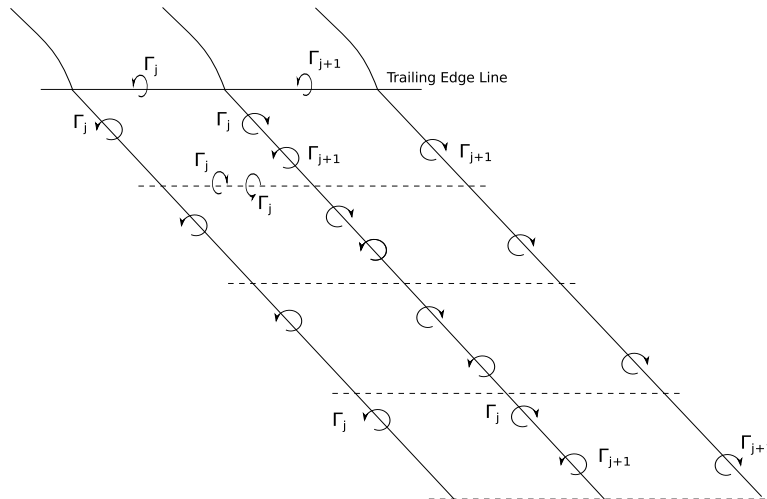


Figure 5.7: Wake with Vortex Rings

There are two distinction in the vortex panels, the ones in the middle of the wake which have active only the vortex in the segments 2 – 3 and 4 – 1 like in Figure 5.8; and those in the first row in which exists the vortex in 1 – 2 too (Figure 5.9), these segments are here maintained because they keep the balance of the wing trailing edge doublets.

The effects make by the elements 3 – 4 in the last row are negligible, their influence in the shape and in the numerical results are so small that they can be omitted in the computation.

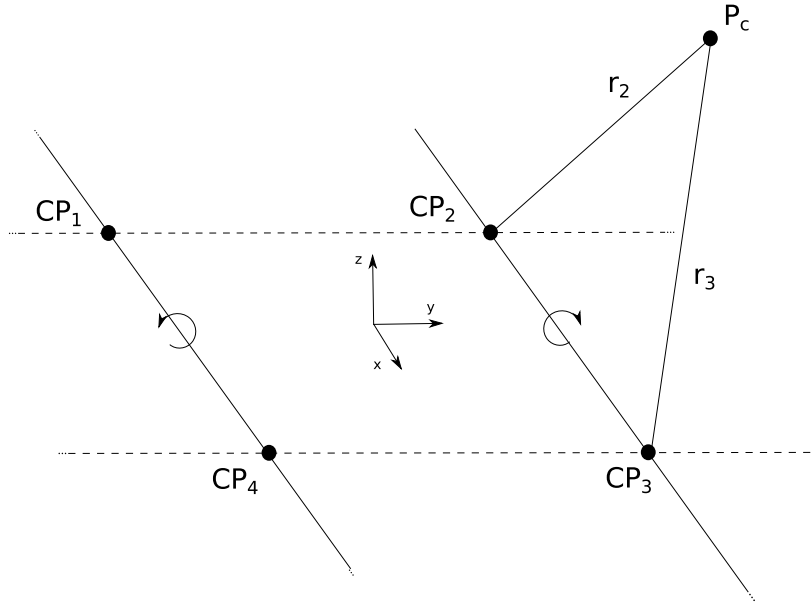


Figure 5.8: General Vortex Panel

Vortex Segment

The utilization of this element follow again what explained in the "Low Speed Aerodynamics" [9], this is represented as Figure 5.10 and produce the induced velocity:

$$V_{ind} = (u, v, w) = \frac{\Gamma}{4\pi} \frac{\mathbf{r}_1 \times \mathbf{r}_2}{|\mathbf{r}_1 \times \mathbf{r}_2|^2} \mathbf{r}_0 \cdot \left(\frac{\mathbf{r}_1}{r_1} - \frac{\mathbf{r}_2}{r_2} \right) \quad (5.9)$$

where $\mathbf{r}_0 = \mathbf{r}_1 - \mathbf{r}_2$

Like the original program, the factor $\frac{1}{4\pi}$ will be omitted avoiding in this way computational errors and saving time.

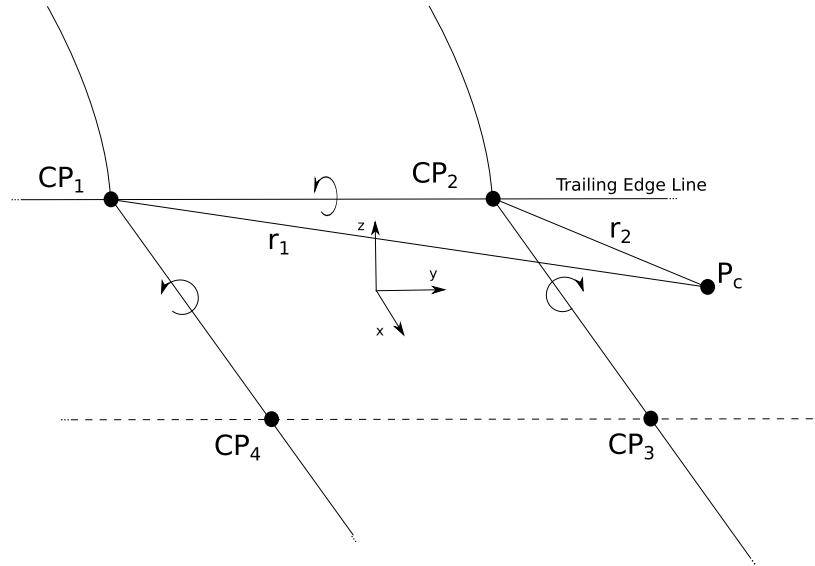


Figure 5.9: First row Vortex Panel

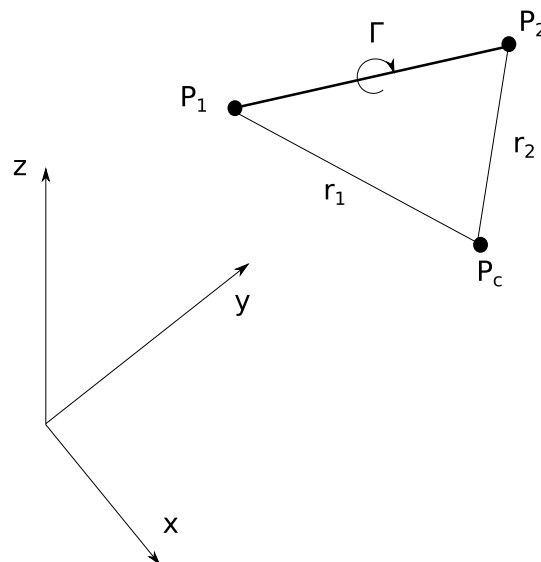


Figure 5.10: Vortex Segment

Singularities Treatment

Figure 5.12 shows how the control points are placed near the nodes of the vortex segment, but one big problem is that this is a place of singularity in which the equation of the velocity produce a value that goes to infinity; furthermore during the relaxation other control points could happen to be near another vortex segment.

A solution to this problem appears to be the employment of a viscous core model on the vortex segment. At first sight this seems to be incompatible with the hypothesis of potential flow models but, as found out in the references [1] and in [17], the panel method is only a mathematical approach for matching the boundary condition and gives a solution for the specific flow field and not a representation of it; this expedient will not invalidate the process, instead is something that help to reach a solution.

The velocities are then modified from the standard Biot-Savart law using the *Lamb-Oseen vortex model* in this way:

$$V_{induced} = V_{B.S.} \left(1 - \exp \left(\frac{-r^2}{r_c^2(t)} \right) \right) \quad (5.10)$$

where:

- r is the radial distance from the vortex element;
- $r_c(t) = \sqrt{4\nu t}$ is the core radius of the vortex ;
- ν is the effective core viscosity.

The time dependency is defined through $t = \frac{x_{TE}}{U_\infty}$, with x_{TE} the distance from the vortex source (trailing edge).

The behaviour of the tangential velocity with the standard vortex equation and with this correction is shown in Figure 5.11, for this example a vorticity $\Gamma = 1$ is used.

It's clear how the velocity near the singularity goes to infinity, instead with the core model it will slowly go to zero, deleting completely the problem. This is useful to avoid an erratic behaviour of the wake.

Other methods to define a vortex core exist, like the Rankine model; but as found in the reference [16], it's said that the Lamb-Oseen is one of the best that can accurate describe the vortex velocity field.

Another method often applied consists in avoiding to take in consideration the self-induced strength of a vortex while the nodes near it are moved.

Note that using a small viscosity and a small offset become the same thing as deleting the self-induction.

With the employment of this modification, when the vortex ring is called one important parameters introduced with the inputs is the *visc_model* logical variable, which is in chief of the activation of the viscous core model

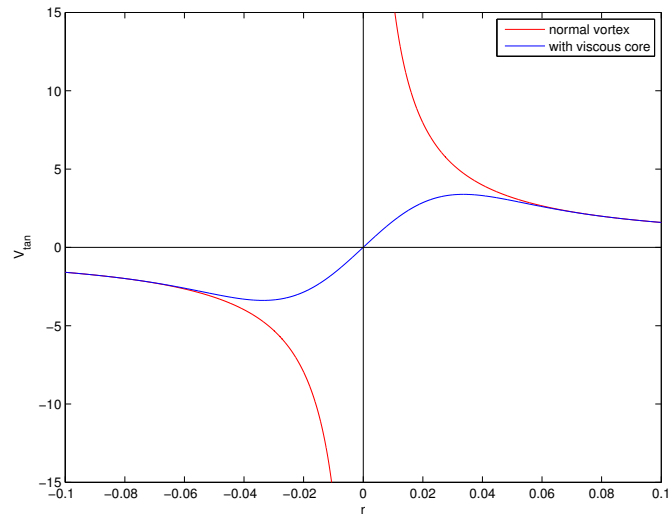


Figure 5.11: Tangential Velocity

correction; the meaning in the use of this variable stands in the two different needs of the wake's properties.

While the process calculates the velocities in the wake control points this is necessary for the reasons just explained, but in the recalculation of the influence coefficients all the wing control points are far enough from the vortex segments, away for any kind of singularity problems made by the vortex rings. Those extra calculations are no longer needed, so the core will not be taken in consideration.

5.6 Definition of the control points

Those are the points in which the induced velocity is evaluated; the relaxation process requires to move the wake nodes so it's chosen to place four of them around each geometric point, two above and two behind the nearby panels.

Corner Points

In the panel method one of the most problematic actions is the definition and the collocation of the control points. Many books and scientific articles talk about the mathematical and physical approach of this method but when it's time to explain about the control points they just speak vaguely about them.

In the relaxation process this is a critical fact, because we need to evaluate the velocities and these depend strictly on the points in which they are calculated.

A solution about how to create the control points in doublet panel corners have been found in the report [8]; from these formulas little changes have been made in order to make the displacement proportional to the local chord like the control points on the wing.

Taking in consideration the point P_4 the four points are calculated from the following expressions:

$$P_c = P_4 + \alpha \hat{D} \quad (5.11)$$

where

$$\hat{D} = \frac{\vec{D}_1 + \vec{D}_2}{|\vec{D}_1 + \vec{D}_2|}$$

$$\vec{D}_1 = \hat{n} \otimes (P_1 - P_4) \quad \hat{D}_1 = \frac{\vec{D}_1}{|\vec{D}_1|}$$

$$\vec{D}_2 = \hat{n} \otimes (P_4 - P_3) \quad \hat{D}_2 = \frac{\vec{D}_2}{|\vec{D}_2|}$$

$$\alpha = \epsilon \times chord$$

Here \hat{n} is the normal in the panel, ϵ the offset choose and chord the local wing chord as said.

Calling the amount of displacement $P_{add} = \alpha \hat{D} = (dx, dy, dz)$, its components are used to create more then one control point like in Figure 5.12

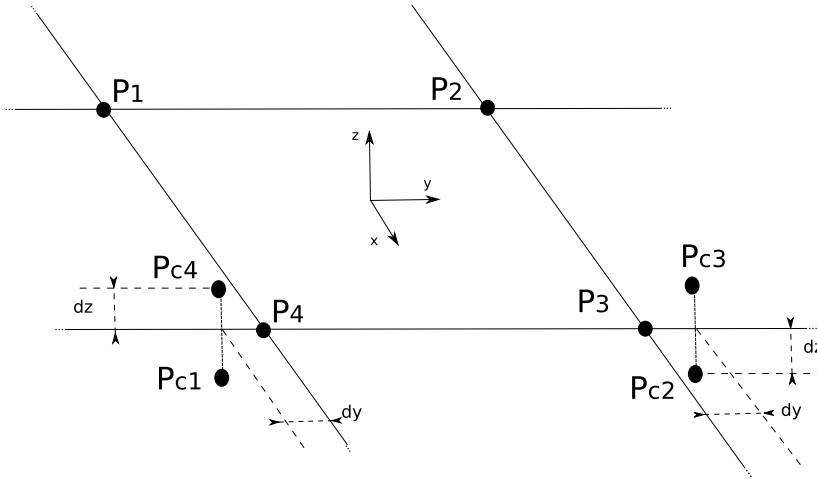


Figure 5.12: Control Points

It's selected to place the P_c at the same x coordinate of the node, so the dx will not be used; then playing with dy and dz the points are created.

Doing this for the row of panels it will produce four control point for each node, see Figure 5.13. In the first and last panel, having no adjacent panel, a couple of extra control points are generated from the same.

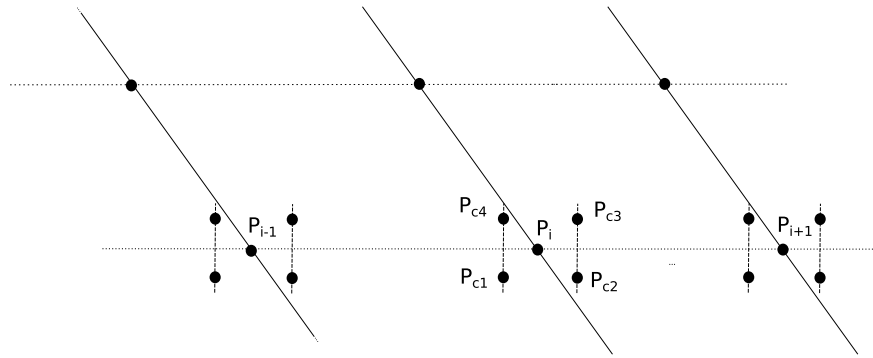


Figure 5.13: Control Points on the Nodes

Midpoints

For the drag integration there's the need to use control points constructed from the midpoints, they are made following the scheme found in the same report as the others point just used:

$$P_c = \frac{1}{2}(P_4 + P_3) + \alpha \hat{D} \quad (5.12)$$

where

$$\vec{D} = \hat{n} \otimes (P_4 - P_3) \quad \hat{D} = \frac{\vec{D}}{|\vec{D}|}$$

$$\alpha = \epsilon \times chord$$

Like before, this is used to create a couple of control points up and down the panel using on time \hat{n} and the other $-\hat{n}$. In order to place them on the Trefftz plane, the component dx will not be used.

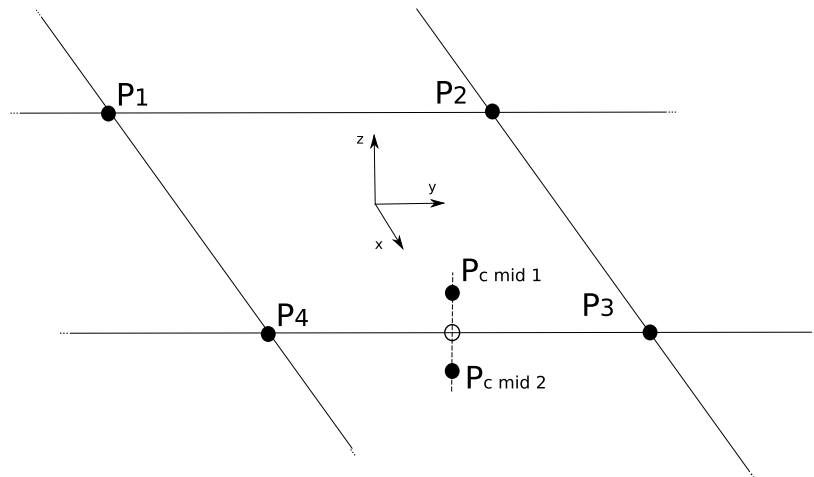


Figure 5.14: Mid Control Points

5.7 Calculation of the Singularities Coefficients

As explained in section 5.2.2 the matrices of the influence coefficients must be redefined each time; but taking a look on the original subroutine used for this purpose and the variables that change in the relaxation process, it can be modified to fulfil in a better way it's goal during the iteration, saving in this way computational time.

By the definition of matrix coefficient follows that this is strictly dependent from the geometry.

The matrix for the source system \mathbf{B}_V remain the same all the time, it depends solely from the wing shape; the case is different for the one defined by the doublet system: $\mathbf{C}_V\textit{strip}$. This is defined by the distribution of doublets both in the wing and in the wake; then the attention must be focus on the possibility to split it in the two origins: $\mathbf{C}_V\textit{strip_wing}$ and $\mathbf{C}_V\textit{strip_wake}$.

So the first one remains always the same as the source matrix, and only the latter needs to be recalculated. For this purpose little change in the original subroutine have been made, separating the doublet treatments and making only the calculation that are really needed.

The strength for the new set of singularities are defined with the standard calls of *PanelStrengths*.

5.8 Integration in Trefftz Plane

This part follows the method that have been described in chapter 4.2.

In the integration a relevant factor has been found; while in the study of the wing aerodynamic properties and the wake shape the value $\frac{1}{4\pi}$ has no influence, in the integration this is relevant. The results order change by a factor of 10^1 ; to give a numerical example takes in consideration the induced drag coefficient integrated with the flat wake:

- without $\frac{1}{4\pi}$: $C_{Di} = 7.903 \cdot 10^{-4}$
- with $\frac{1}{4\pi}$: $C_{Di} = 9.932 \cdot 10^{-3}$

The second one seems to be more reasonable with the value obtained from the Lifting Line Theory (see chapter 6.3).

The intentions in this project are only the treatment of the wake and its integration; so, without trying to change the choices in the wing program, will be introduce two subroutine that correct the values obtained: *Correction_4pi_Strengths* and *Correction_4pi_Vel*.

So before entering in the *DragIntegration* the previously influence coefficients are modified and the new singularity strengths calculated; in the same way inside the subroutine the velocities are corrected before being used

in the calculation.

Then the integration can be achieved.

Chapter 6

Final Results

The way suggested to check the validation of the program written and the drag calculated, consists in the verification of the coefficient obtained from a simple wing with its theoretical value.

6.1 Introduction to Prandtl's Theory

Applying the *Prandtl's Lifting Line Theory* the aerodynamics properties of a wing could be calculated; for ours purpose only the induced drag definition is needed, and we will focus on its evaluation.

The complete explanation of this can be found in all the major aerodynamics books like those in references [3] and [10].

As briefly exposed in 2.2.1, an actual finite wing can be defined with a superposition of horseshoe vortex elements of various strengths as in Figure 6.1.

Known the vorticity distribution $\Gamma(y)$, lift, induced drag and induced drag coefficient can be evaluated:

$$\begin{aligned} L &= \rho_\infty V_\infty \int_{-b/2}^{b/2} \Gamma(y) dy \\ D_i &= \rho_\infty V_\infty \int_{-b/2}^{b/2} \Gamma(y) \alpha_i(y) dy \\ C_{D,i} &= \frac{D_i}{q_\infty S} = \frac{2}{V_\infty S} \int_{-b/2}^{b/2} \Gamma(y) \alpha_i(y) dy \end{aligned} \tag{6.1}$$

Where α_i is the induced angle of attack.

The condition of minimum drag is achieved through an elliptical distribution of vorticity:

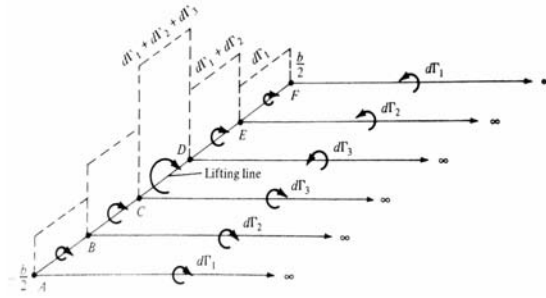


Figure 6.1: Prandtl's lifting line theory

$$\Gamma(y) = \Gamma_0 \sqrt{1 - \left(\frac{2y}{b}\right)^2}$$

that leads to write:

$$\begin{aligned} L &= \rho_\infty V_\infty \Gamma_0 \frac{b}{4} \pi \\ \Gamma_0 &= \frac{4L}{\rho_\infty V_\infty b \pi} \\ \Gamma_0 &= \frac{2V_\infty S C_L}{b \pi} \end{aligned} \quad (6.2)$$

With this lift distribution the induced angle of attack is constant along the span, and it could be written as:

$$\alpha_i = \frac{C_L}{\pi AR} \quad (6.3)$$

Substituting eq. (6.2) and (6.3) into (6.1) produce:

$$C_{D,i} = \frac{C_L^2}{\pi AR} \quad (6.4)$$

As said, this is valid only for an hypothetical elliptical distribution that it's not achieved every time. This must be generalised for any other lift distribution.

The generic form of the drag coefficient is:

$$\begin{aligned} C_{D,i} &= \frac{C_L^2}{\pi AR} (1 + \delta) \\ &= \frac{C_L^2}{e \pi AR} \end{aligned} \quad (6.5)$$

where the variable e is called *span efficiency factor*.

The values assumed are always $e \leq 1$; the condition $e = 1$ it comes in the case of elliptical lift distribution, here the drag will have the minimal value and this is the reason why this kind of distribution is normally sought.

6.2 Span efficiency

The values of e depend only on the wing geometry and in many book it could be found the graphical function of δ with the variation of AR and the ratio of root and tip chord. But those are small graphics in which it's hard to pull out a correct information; the solution seems to calculates this parameters from the start.

This is explained in many book, what will be applied now follows what found in "Foundation of Aerodynamics"[3] when it describes the behaviour of an arbitrary circulation distribution of vorticity.

It starts with a representation with a Fourier series of the arbitrary symmetrical circulation distribution

$$\Gamma = \frac{1}{2}m_0s c_s V_\infty \sum_{n=1}^{\infty} A_n \sin(n\theta) \quad (6.6)$$

the subscript s define the values on the symmetry plane, c it's the chord and m_0 is the slope of the graphic $C_l - \alpha$ of the airfoil.

Some passages here are avoided, if interested the could be easily found in the book.

The expression of the angle of attack is written:

$$(\alpha - \alpha_{L=0}) = \frac{c_s m_{0s}}{c m_0} \sum_{n=1}^{\infty} A_n \sin(n\theta) + \frac{c_s m_{0s}}{4b} \sum_{n=1}^{\infty} n A_n \frac{\sin(n\theta)}{\sin(\theta)} \quad (6.7)$$

an expression of the induced drag coefficient become:

$$C_{Di} = (C_{Di})_{elliptic} \sum_{n=1}^{\infty} \frac{n A_n^2}{A_1^2} \quad (6.8)$$

with

$$\begin{aligned} (C_{Di})_{elliptic} &= \frac{C_L^2}{\pi AR} \\ C_L &= \pi^2 \frac{A_1}{2} \end{aligned} \quad (6.9)$$

eq. (6.8) is rewritten:

$$C_{Di} = (C_{Di})_{elliptic}(1 + \delta) \quad (6.10)$$

where:

$$\delta = \sum_{n=2}^{\infty} \frac{n A_n^2}{A_1^2} \quad (6.11)$$

So the solution of the problem become find out all the coefficients A_n .

Evaluation of the coefficients A_n

Working with a rectangular wing build with the same profile makes the things easier, the chord and the slope will not change in the span-wise direction.

The infinite series will be stopped at a chose value of n , then the equation (6.7) must be satisfied at each $\theta = \cos^{-1}(2y/b)$. Having halted the series, and due to the symmetry, n station point θ_0 are defined on one half of the span. In this way the equation produces the system:

$$[a]\{A_n\} = \{\alpha\} \quad (6.12)$$

that can be solved for the unknown A_n .

6.3 Wing for validation

It's chosen to deal with a rectangular wing with no swept or dihedral angle, the sections are made with symmetric profile.

The wing used has the following properties:

- AR = 4
- c = 500
- span = 2000
- $\alpha = 5^\circ$
- profile NACA 0015

The choice of symmetrical airfoils makes simplification in the calculation of the coefficients A_n in eq. (6.7) :

- $c_s = c$
- $m_{0s} = m_0$
- $\alpha_{L=0} = 0^\circ$

Note that $m_0 = 2\pi$ from the theory of the profile explained in [10].

For the calculation of the factor δ explained in the previously section, a little matlab program for the generic Lifting Line has been made. The results have been compared with the examples shown in "Foundations of Aerodynamics" [3] and they agree with them; to reach a better definition of the data the Fouries series is defined using a $n = 1000$; use higher values make no better resolution.

So following eq. (6.8), (6.9) e (6.11) the values found are:

- $\delta = 0.028476875151218$

- $C_L = 0.351543059967817$
- $(C_{Di})_{elliptic} = 0.009834384708527$
- $C_{Di} = 0.010114437254061$

The span efficiency become $e = 0.972311603849108$

6.3.1 Testing the Subroutine

To proof the right operation of the drag integration its subroutine has been first tested with the flat wake (Figure 6.2), obtaining as result $C_{Di} = 1.0005 \cdot 10^{-2}$.

This is enough near the expected one to reassure on the accuracy of the relaxed wake integration.

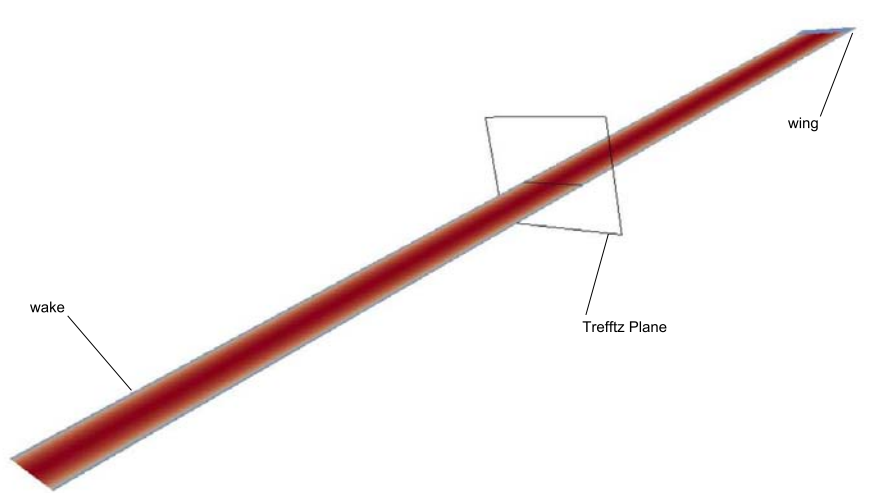


Figure 6.2: Flat Wake Integration

6.4 Results

The result of the drag integration is strictly dependent to the geometry reached; but this is not so simple to achieve.

As described in chapter 5.5.2 a way to solve the singularity problem is the viscous core; but this is also something that must be taken in highly consideration.

The value chosen for the viscosity ν modify the core radius length (Figure 6.3); so this will become a way to define the space region of the vortex segment influence, this is a factor that has a strongly effect on the converged shape; as found in reference [12] a solution could be making this parameter varying and examine its effects.

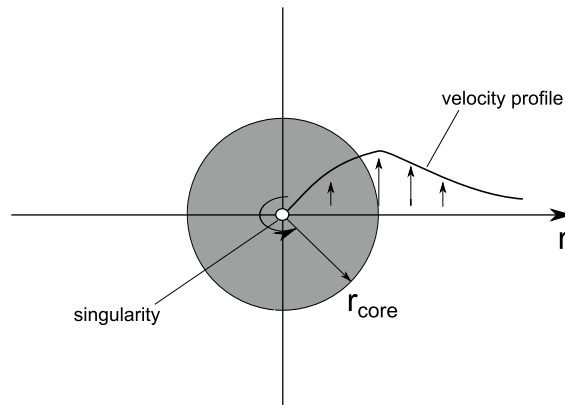


Figure 6.3: Core Radius

Radius Core Influence

Taking fixed the value of the wake paneling and the control points offset, in the Figure 6.4 and 6.5 is shown the effect made by different values of the viscosity.

But despite the good section the drag coefficients evaluated are merely the half of the expected value.

In Figure 6.6 is shown the behaviour of the C_{Di} calculated with the variation of the core dimension; from some point the shape starts to act strange and the panels to cross themselves, maybe because the control points are no longer well treated from the singularities, and the results leak in reliability, as example the shape in Figure 6.5(b) defined a result of $C_{Di} = 9.251 \cdot 10^{-3}$.

The coefficient increase with the core decreasing; but with it the penetration shown up.

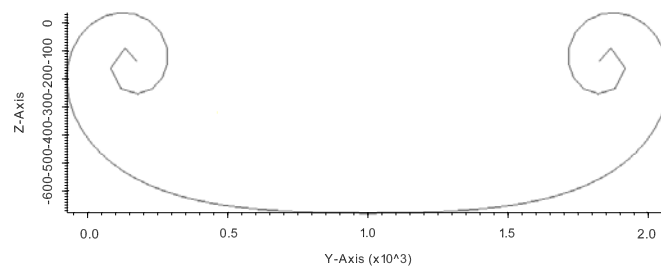
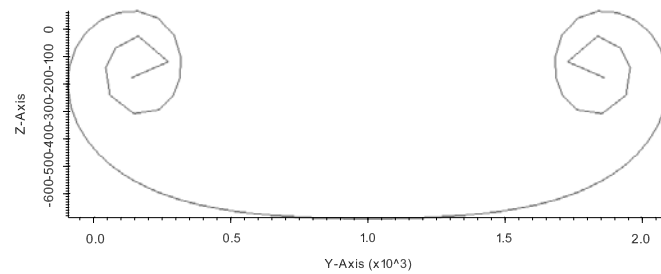
Trying not to use the viscous model but instead deleting the self-induction, the shape is the one in Figure 6.5(c), but downstream the wake presents interpenetration, it has produced $C_{Di} = 5.114 \cdot 10^{-3}$.

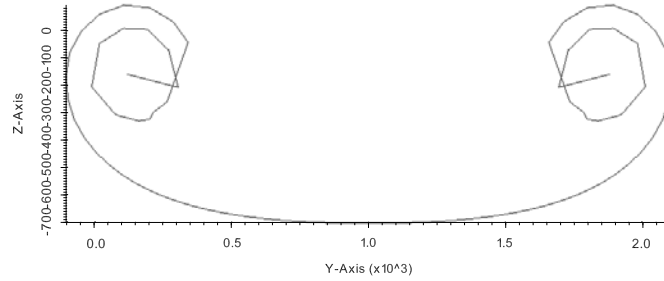
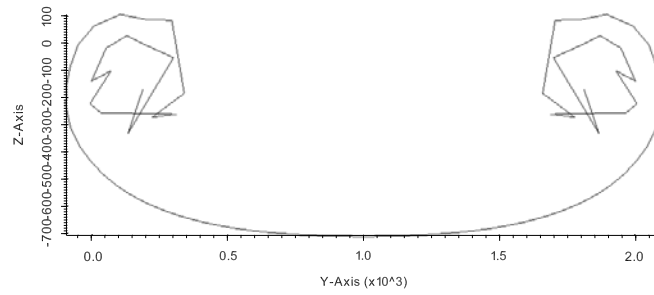
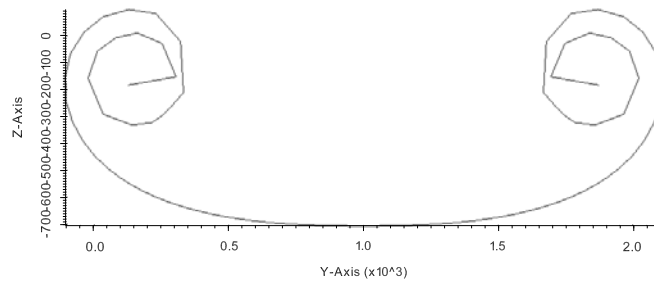
Offset Influence

It could be interesting observe the influence of the offset given to the control points respect of a fixed radius core.

It's setted to use the values $1e^{-2}$, $1e^{-3}$, $1e^{-4}$ and $1e^{-5}$; the result trend is shown in Figure 6.7.

With small cores the coefficient increases with the control point approaching. But in both simulations the penetration problem remains the same.

(a) $\nu = 1$ (b) $\nu = 0.5$ **Figure 6.4:** Radius Core Influence on the Shape a

(a) $\nu = 0.1$ (b) $\nu = 0.01$ 

(c) Without self-induction

Figure 6.5: Radius Core Influence on the Shape b

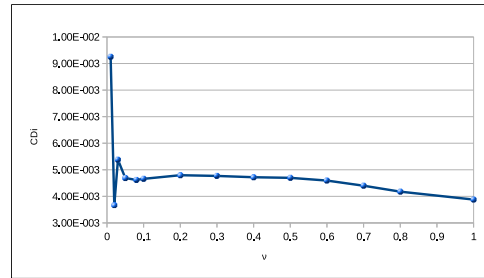


Figure 6.6: Radius Core Influence on C_{Di}

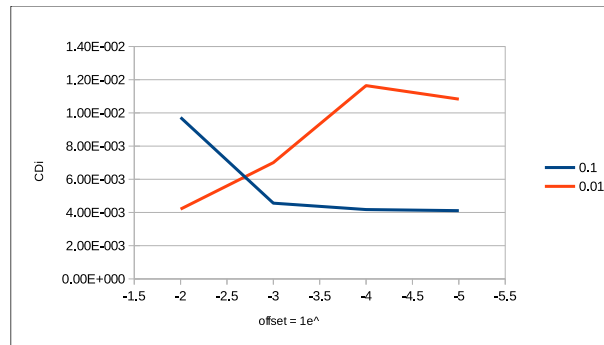


Figure 6.7: Offset Influence

Panels Influence

Now, the value for the core model is fixed at $\nu = 0.5$, the wake discretization is made to vary in such a way to be able to observe its influence on the wake shape and the drag coefficient achieved.

In Figure 6.8 and reffig:prove 0.5 b are shown some results, the title of each figure represents the schematization according to chapter 5.4.1. Figure 6.9(b) is made with an offset of $1e^{-1}$, the others with $1e^{-2}$; smaller ones make no differences.

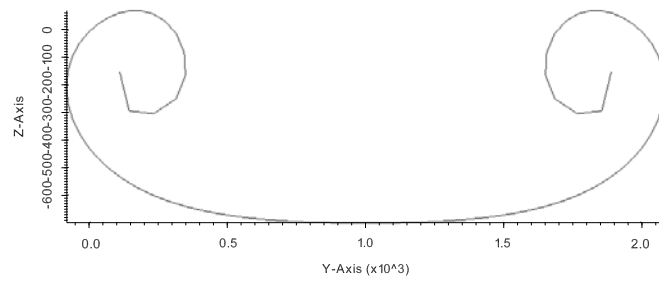
In the firsts three the geometry maintain itself good, with the increase of panels it's even able to roll-up itself a discrete number of time without any problem. The last one instead presents interpenetration. But, even though this good behaviour, the integration doesn't produce the hoped values:

(a) $C_{Di} = 4.23 \cdot 10^{-3}$

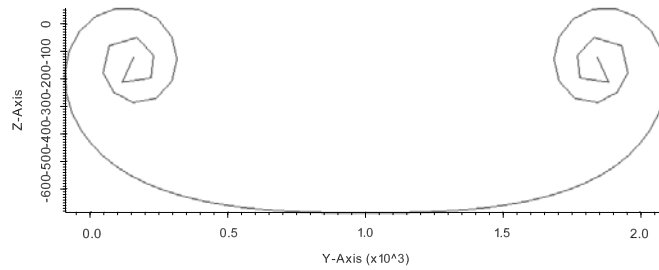
(b) $C_{Di} = 5.07 \cdot 10^{-3}$

(c) $C_{Di} = 4.76 \cdot 10^{-3}$

(d) $C_{Di} = 2.91 \cdot 10^{-3}$

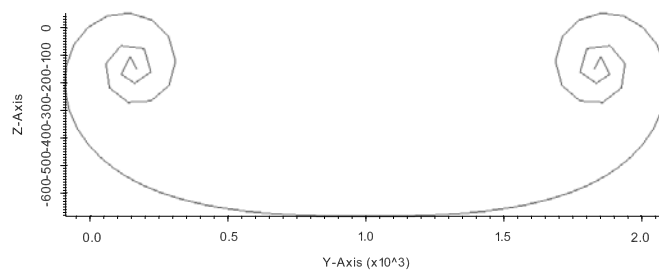


(a) 1-10-10-10

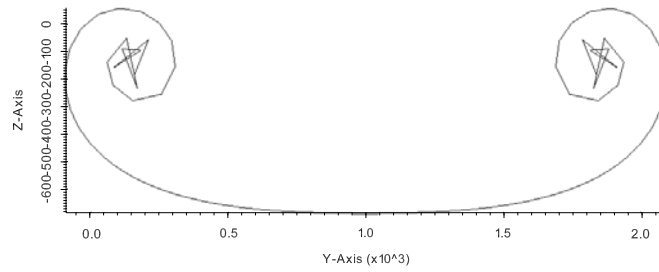


(b) 10-40-40-20

Figure 6.8: Panels Influence on the Shape a



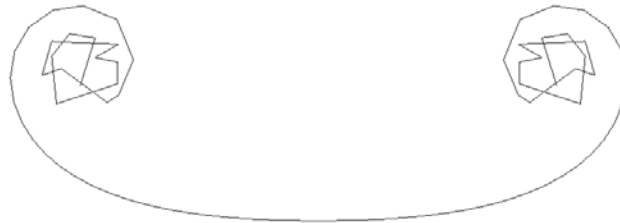
(a) 20-100-100-20

(b) 10-40-40-20 offset $1e^{-1}$ **Figure 6.9:** Panels Influence on the Shape b

Others attempts have been made with smaller value for the core. But now biggest problems are born: the presence of the panels interpenetration. Changing the number of panels used and the offset of the control points seems to produce no kind of benefits in the geometry; this panels intersection manifests itself in most of the simulation, and despite such problem, with the increase of the rows the integration produce results near the right one. The sections in Figure 6.10 are made with a $\nu = 0.01$, and the produced:

(a) $C_{Di} = 1.082 \cdot 10^{-2}$

(b) $C_{Di} = 1.188 \cdot 10^{-2}$



(a) 10-50-50-20 offset $1e^{-3}$



(b) 10-40-40-20 offset $1e^{-5}$

Figure 6.10: Sections with correct C_{Di} 1

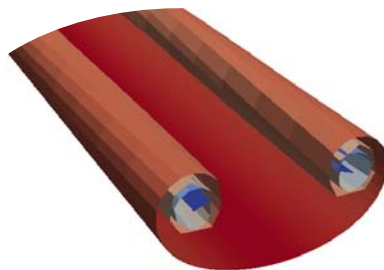
Instead, trying with simply avoiding the self-induced vorticity (note again that it's equal to use small core and small offset) the problem manifested itself once more.

Attempting to seek a reasonable shape (like in Figure 6.11) with different panel lengths the perforations always shown up; while the initial roll-up seems to produce a good shape, downstream this attitude won't never be maintained.

Moreover, like before the integration presents correct values with the presence of penetrations (see Figure 6.12).



(a) $C_{Di} = 6.129 \cdot 10^{-3}$



(b) Downstream penetration

Figure 6.11: "Correct Shape" with no self-induction

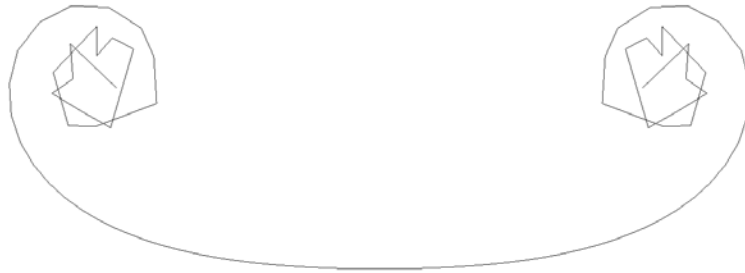
Points Integration Influence

In the program has been inserted another method to evaluate the point positions, one based on the trapezoidal rule 5.1.1.

With an iterative process one problem could be the propagation of the numerical errors, and this 2-step method has a higher reliability than the Euler 1-step.



(a) $C_{Di} = 1.0001 \cdot 10^{-2}$



(b) $C_{Di} = 1.1870 \cdot 10^{-2}$

Figure 6.12: Sections with correct C_{Di} 2

The negative side is the computational time, with the supplement of the second step the calculation time is doubled and this could be relevant in complex analysis.

Nevertheless, it has been applied with the same conditions used in the Figures 6.4(b), 6.5(a) and 6.10(a); the shapes achieved are compared in Figure 6.13.

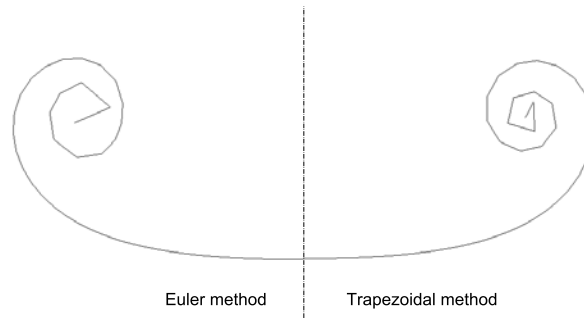
With the biggest core the wake achieves a higher roll-up, but in the others cases the interpenetration seems to be enhanced. The coefficients calculated remain similar of the ones made by Euler method.

6.5 Attempts with complex geometry

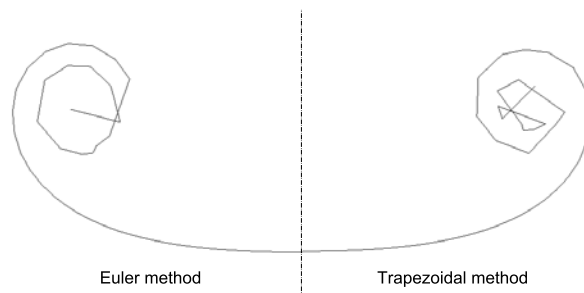
Now program has been applied with an arbitrary non-planar wing, despite the well known wrong results; it's setted with the same conditions that in the previously example made a "good geometry".

With a C-wing in Figure 6.14, the wake convected itself as in Figure 6.15 where there are the sections made in different positions. Figures 6.16 and 6.17 show the results with a winglet.

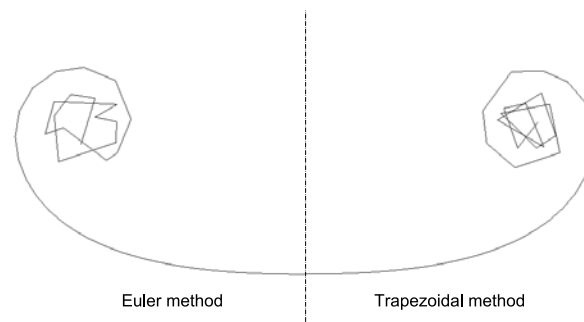
Now the geometry doesn't remain acceptable on its entire length, even if with the simple wing there were no kind of problems; the wake seems to create more than one vortex region, that the continuous geometry can't describe properly and again the interpenetration problem presents itself once more.



(a)



(b)



(c)

Figure 6.13: Points Integration Influence on the Shape

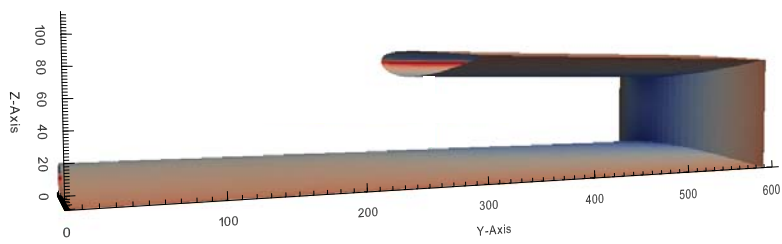


Figure 6.14: C-Wing

(a) Section $2 \frac{b}{2}$ (b) Section $4 \frac{b}{2}$ 

(c) Section Trefftz Plane

Figure 6.15: C-Wing Wake's Sections

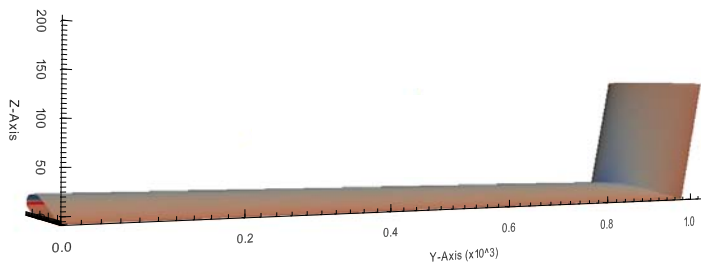
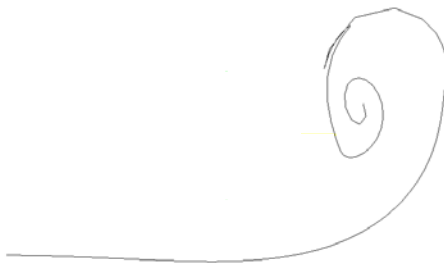


Figure 6.16: Wing with Winglet

(a) Section $2 \frac{b}{2}$ (b) Section $4 \frac{b}{2}$ 

(c) Section Trefftz Plane

Figure 6.17: Wing with Winglet Wake's Sections

Chapter 7

Final Comments

The assumption of the viscous core seems to be the best way to produce a wake with a good shape, able to show the roll-up effect; but this geometry is not enough to allow the exact integration of the induced drag coefficient through the Trefftz plane; the high radius core value is unrealistic in a real flowfield.

The geometry is highly influenced by the reduction of the core radius, or by the avoiding of the self-induction, and following this path the integration result become nearer the theoretical ones; but with it the problem of panel interpenetration become relevant.

This phenomenon is something that could shown up in the panel method; as an example in the reference [1] the shape achieved in Trefftz plane is the one in Figure 7.1; and, again despite the problem, it produce a right value for the drag coefficients, but the penetration isn't considered as a "problem that invalidate the results".

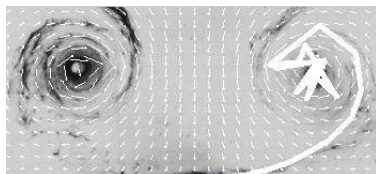


Figure 7.1: Interpenetration Problem

In the reality from a vortex element there is a transition region where the fluid goes through a turbulent state before sets itself into a laminar one. This is a phenomenon that is not taken in consideration in an inviscid study and its influence in the seeking of the real shape could be relevant.

The singularity treatments through a core radius is only a way to avoid the infinity problem, and not something that can simulate the real comportment of a fluid.

Panels that end up crossing themselves shouldn't be something realistic, they represent a material region; so the acceptability of those results haven't

enough reliability.

Appendix A

Description of the Subroutines

Here a list of the subroutine created and modified with a brief description

A.1 Subroutines Modified

This thesis is an implementation of a program written by Dipl.-Ing. Uwe Schuster, so few subroutines have been modified to be adapted to the relaxation scheme.

The titles of the paragraphs represent the name of the relative subroutine

Source_velocity

Given that in different points of the program there's the need of the calculation of the velocities, to be able to do this simpler all the row of codes concern the source panels have been gathered in a single block.

Wing & Wake QuadrilateralDoubletStrip

The original treatment of all the doublet have been change for the same reason as the source system and for the motivation explained in 5.7.

The first collects all the equations and subroutines needed to calculate the velocity component due to the wing's doublet distribution, the second one is instead used just for the wake's doublet.

IntroducePanels

The only modification here made consists in adding the vector \mathbf{P} in the output, those points are used in the creation of the control points.

InfluenceCoeff

As explained in 5.7 the calculation of the matrix have been separated in its two components, and the *C_V_strip_wing* is added to the output variables to be used in the next recalculation of the coefficients.

A.2 Subroutine Created

GKS_to_VCS

This is the subroutine that make the change in the coordinate system (5.3; it sized the input vector, calculates the rotational matrix for the defined angle and than makes the multiplication to obtain the vector in the new frame.

Wake_Relaxation

This is the main part of program for the convection process. It required for input the wing geometry and the variables for the panel method analysis. For the process are also introduced the offset of the control points, the complete length of the wake and the position of the Trefftz plane. Inside are defined the variable in charge for the convergence, tolerance saves step. The procedure begins creating the initial conditions on geometry and singularities distribution. Logical variables *mu_recalc*, *test_RK2* define the way to go on with the iteration.

The output variables will be of course the new wake configuration with the all others needed for the remain part of the program that analyzes the wing's aerodynamics properties.

While the iteration is going on, on the display will be shown at each step the maximum displacement done, the tolerance chosen and the change in the doublets shed in the wake.

Zero_WakePoints

Once the paneling properties are setted (chapter 5.4.1) this starts to create the geometry of the "zero wake" from which begin the iteration. It scans the *AdvWingPoints* to get the reference coordinate to place the Trefftz plane; with the variables imposed for the paneling starts to calculate all the geometric characteristics and starts to build up row by row all the wake's nodes.

The output is represented with the vector *WakePoints* and the location within it of the points that make the intersection with the plane (*ii_TP*).

Semispan_calc

It's a simple subroutine that define the semispan; it creates a vector with all the y-coordinate of the trailing edge wing points and finds the maximum value in it. This represents the span of or the semispan if it's true the symmetry condition.

Control_Point

Giving in input the the geometric informations of a panel (points P and rotation matrix) and the ones for the offset (local chord ad offset quantity) this subroutine defines the displacements P_{add} needed to creates the control points in the panel's nodes, as explained in 5.6.

Define_Control_Point

This is where all the control points are created.

For the the specific row in the iteration the panels in analysis are individuated for the call of the previously subroutine and then for all the nodes P_4 and P_3 the control points are produced as described again in 5.6.

In the end the output will be a vector in which are defined the four control points for all the geometric wake's nodes in the row.

VelocitiesCalculation

This subroutine is the one headed to the calculation of the velocities induced by the source, wing's doublets and wake's vortex rings system; it's created to work with a set of control points as input. This is sized and then a do cycle begin to calculate the velocities for each point.

Define_velocities

Here the velocities in the wake's nodes are defined. The major inputs are the control points made in *Define_Control_Point* and the infinity velocity; in each geometric points it's associated the average of the velocities calculated through *VelocitiesCalculation* and then the U_∞ is added to obtain the complete velocity.

Displacement_Eulero

In this subroutine the integration of the nodes displacement takes place; it follows the Euler scheme.

The inputs are represented by the vector with the wake points and the velocities previously evaluated. Then the next point position is evaluated for the entire row following (5.1) and the displacement achieved is imposed

to the all points downstream, recreating in this way the new wake geometry and replacing the old coordinates in *WakePoints*.

This subroutine also check the majors displacement in both y and z -coordinate and then the biggest one, this value *d_max* is used for the convergence control.

C_V_strip_Recalculation

This follows what described in 5.7 the matrix *C_V_strip_wake* related to the new wake geometry is calculated anew and added to *C_V_strip_wing* to create the new *C_V_strip* in order to update the singularities.

Mu_TE_Calculation

As the name says its aim consists in calculate the doublet intensities μ spread from the trailing edge to the wake. The major use of this subroutine is related to the convergence about the singularities, when after a complete movement the difference from the previously iteration is calculated and checked in the convergence loop.

Wake_visc_VortexRing

Here we take count of the wake's doublet, as explained in chapter 5.5 the panels are treated as *Vortex Rings* in the way described. The logical input *visc_model* set the choice of the use of the viscous core to avoid the singularity problem.

CorrectWakePanels

It follows the scheme of the original *IntroducePanels* and upgrades all the wake panel properties after each movement.

Correction_4pi_Strengths

As the name says and as has been explained in chapter 5.8 this will correct the coefficients calculated.

The inputs consist in the two matrices *B_V* and *C_V_strip*, these will be sized and then the components are modified with the product $\frac{1}{4\pi}$; the new output matrices are so created.

Correction_4pi_Vel

This works in the same way as the previous one, the input is the velocity vector which includes all the row nodes velocities calculated, it sizes it and corrects the elements with the $\frac{1}{4\pi}$ factor.

Drag_integration

In this subroutine the integration in the Trefftz plane take place, it follows what explained in the chapter 4.2. The index *ii_TP* is finally used here to catch the points in the plane.

Now the control points are based from the mid points, the displacements to add for their construction are calculated from the formulas shown in 5.6. For the integration, at the mid points are associated again the average of the two velocities. The jump in the singularities is defined through the *Mu_TE_Calculation*.

The application of the trapezoidal rule needs the distance between nodes, this follows the length of the wake (see chapter 4.2)

Drag_Integration_Surface

This is a try on application of the surface integral from (4.14).

First_Wake

This is different way to make the first iteration, some articles like [4] suggests that in the beginning it could be suitable to displace the nodal points taking in consideration only the upstream system influence. The singularities are recalculated after a chosen interval.

Upstream_Wake

Here a copy of the wake is made, but taking in account the upstream elements.

Displacement_Trapezoidal

This one is in charge to compute the next point position with the other method explained through the eq. (5.2).

Step_Wake

Here all the variables of the wake and of the panels are cloned for the first step of the RK2; otherwise the properties from the previously iteration will get lost.

Read_WakePoints \$ Read_singularities

The program saves in files .dat with the wake and singularities results, those subroutine are build in order to read those data and recreate the vector for the analysis.

Bibliography

- [1] *A Higher Order Vortex-Lattice Method with a Force-Free Wake*. PhD thesis, The Pennsylvania State University, 2006.
- [2] Anmar H. Ali. Wake roll-up behind wings with ground effect. *The Iraqi Journal For Mechanical And Material Engineering*, vol. 10, no. 2, pp. 182-202, 2010.
- [3] Chuen-Yen Chow Arnold M. Kuethe. *Foundation of Aerodynamics*.
- [4] A. Plotkin D.T. Yeh. Vortex panel calculation of wake roll-up behind a large aspect ratio wing. *AIAA Journal*, vol. 14, no. 9, pp. 1417-1423, 1986.
- [5] L. Morino E. O. Suci. A non linear finite element analysis of wings in steady incompressible flows with wake rollup. Technical report, AIAA, 1976.
- [6] I. Parschivoiu F. Lamarre. Efficient panel method for vortex sheet roll-up. *AIAA Journal*, vol. 29, no. 1, pp. 28-33, 1992.
- [7] M. D. Maughmer G. Bramesfeld. Relaxed-wake vortex-lattice method using distributed vorticity elements. *AIAA Journal*, vol. 45, no. 2, pp. 560-568, 2008.
- [8] Forrester T. Johnson. A general panel method for the analysis and design of arbitrary configurations in incompressible flows. Technical report, NASA, 1980.
- [9] Allen Plotkin Joseph Katz. *Low Speed Aerodynamics 2nd Edition*.
- [10] John D. Anderson Jr. *Fundamentals of Aerodynamics*.
- [11] Ilan Kroo. Highly nonplanar lifting systems. Technical report, NASA, 1995.
- [12] S. L. Mondolini. *A numerical method for modelling wings with sharp edges maneuvering at high angles of attacks*. PhD thesis, MIT, 2001.

- [13] I. M. Kroo S. C. Smith. Computation of induced drag for elliptical and crescent-shaped wings. *AIAA Journal*.
- [14] I. M. Kroo S. C. Smith. Induced drag computation on wings with accuray modeled wakes. *AIAA Journal*, vol. 34, no. 2, pp. 253-255.
- [15] Uwe Schuster. *Entwicklung eines Programmmoduls zur Berechnung der Auftriebsverteilung von Flugzeugtragflächen mit Hilfe einer 3D Panel-methode*. Number ILR/LFT G 10-20. Technische Universitaet Dresden, Institute of Aerospace Engineering, 2010.
- [16] Nilay Sezer-Uzol. *High accuracy wake and vortex simulations using a hybrid Euler/discrete vortex method*. PhD thesis, Pennsylvania State University, 1993.
- [17] Stephen C. Smith. A computational and experimental study of nonlinear aspects of induced drag. Technical report, NASA, 1996.